

# **Calibration of a catchment-based land surface model in the Loire River basin (France) to assess hydrological impacts of climate change**

François Bourgin

Paris, November 2009

under the supervision of Dr. Agnès Ducharne

A thesis submitted to the Technische Universität München (TUM)  
for the degree of Master of Science in Environmental Engineering

## Abstract

This thesis contributes to the ICC-HYDROQUAL project whose aim is to investigate climate change impacts on water resources in the Loire River basin (around 110 000 km<sup>2</sup>), one of France's main river basins. This study uses the Catchment LSM (CLSM), a semi-distributed land surface model that describes the coupled water and energy budgets based on near-surface meteorology. The CLSM uses the concept of TOPMODEL to account for lateral water fluxes along topography and their influence on the small scale variability of soil moisture, runoff and evapotranspiration. The main purpose of this study was to calibrate the CLSM in the Loire basin (subdivided into 68 unit catchments). The performance of the CLSM was determined by comparing the simulated runoff to observed river discharge. To ensure that the model correctly captures the overall behavior of the basin, an independent evaluation of model performance was carried out, using the classical split-sample method. Additionally, a sensitivity analysis of the model to two soil parameters, the soil depth and the wilting point, was conducted and several interesting points were outlined, which could contribute to a better understanding of how the CLSM simulates the soil moisture control with respect to evapotranspiration.

## Acknowledgements

My first thanks go to Dr. Agnès Ducharne who offered and supervised this research project. I very much appreciate her support and advice, as well as the liberty she gave me to explore my ideas. I also owe special thanks to Prof. Erwin Zehe, whose lectures at TU München introduced me to, and more important made me interested in hydrological sciences.

I am grateful to the people working at the UMR Sisyphe, especially Prof. Pierre Ribstein, the PhDs students next door and of course Meriem Labbas, for their welcoming attitude.

Last but not least, I would like to thank Prof. Laurent Mortier and the ENSTA Paris-Tech International Office for kindly supervising and supporting me while I was abroad.

# Contents

<b>1</b>	<b>Introduction</b>	<b>1</b>
1.1	Context . . . . .	1
1.2	The ICC-HYDROQUAL project . . . . .	2
1.3	Objectives of this thesis . . . . .	2
<b>2</b>	<b>Model description</b>	<b>4</b>
2.1	Land surface modelling . . . . .	4
2.1.1	Background . . . . .	4
2.1.2	Evolution of land surface models . . . . .	5
2.2	The Catchment Land Surface Model (CLSM) . . . . .	6
2.2.1	Soil moisture variability . . . . .	7
2.2.2	Spatial partitioning within the catchment . . . . .	9
2.2.3	Energy and water budgets . . . . .	11
2.2.4	Validation and applications . . . . .	13
<b>3</b>	<b>Modelling the Loire River basin</b>	<b>14</b>
3.1	Study site and data description . . . . .	14
3.1.1	The Loire River basin . . . . .	14
3.1.2	Data sources . . . . .	14
3.2	Modelling results . . . . .	17
3.2.1	Calibration strategy . . . . .	17
3.2.2	Analysis of results . . . . .	19
3.3	Sensitivity analysis . . . . .	25
3.3.1	Motivation . . . . .	25
3.3.2	Sensitivity to the soil depth . . . . .	26
3.3.3	Sensitivity to the wilting point . . . . .	33
3.3.4	Discussion . . . . .	36

---

<b>4 Conclusion</b>	<b>40</b>
4.1 Summary . . . . .	40
4.2 Perspectives . . . . .	41
<b>A Appendices</b>	<b>43</b>
A.1 Study site and characteristics of the unit catchments . . . . .	43
A.2 Modelling results . . . . .	46
<b>Bibliography</b>	<b>52</b>
<b>List of Figures</b>	<b>58</b>
<b>List of Tables</b>	<b>60</b>



# 1 Introduction

## 1.1 Context

Freshwater resources are among the systems that are particularly vulnerable to climate change (Bates et al., 2008). Changes in precipitation patterns affect water availability and runoff directly, while changes in temperature, radiation and humidity have an effect on evapotranspiration. Predicting the potential effects of anthropogenic climate change on water resources is critical for policy makers and water management, especially since business as usual is no longer possible (Milly et al., 2008).

Global climate models (GCMs) are invaluable tools for characterizing the sensitivity of climate to anthropogenic forcing. Projections of these models can help to determine the perturbations in the global water cycle that are expected to accompany climate warming (Milly et al., 2005). In Europe for instance, projected mean annual precipitation is generally expected to increase in northern Europe and to decrease further south (Bates et al., 2008). However, despite considerable improvements, GCMs still contain large errors, due to simplification of climate representation, potentially wrong assumptions about climate processes and limited spatial and temporal resolution. GCMs are currently not able to properly quantify the impacts of climate change at the regional scale, which is the relevant scale from the practical point of view of policy-making decisions.

Therefore, a combination of climatic, hydrologic and ecological models is often used in climate change impact studies. The main steps of such studies are: (1) construction of emission scenario; (2) global climate modelling; (3) downscaling; (4) impact modelling (Boe et al., 2009). Each step involves uncertainties and errors that may propagate in a very complex way. This modelling framework is in particular well established in the French scientific community. Several regional impact assessment studies have used GCMs results as input for their models (Etchevers et al., 2002; Caballero et al., 2007; Ducharne et al., 2007). In these studies, uncertainties are taken into account by considering either different emissions scenarios, different GCMs, different downscaling methods

or different hydrological models. In the more recent RExHySS project (Ducharne et al., 2009b), which aimed at assessing the impact of climate change on the water resources and hydrological extremes of the Seine and Somme river basins, eight climate simulations, downscaled by three different methods, were used to drive five hydrological models.

## 1.2 The ICC-HYDROQUAL project

The ICC-HYDROQUAL project, supported by the “Plan Loire Grandeur Nature”<sup>1</sup>, started at the beginning of 2009. Its main purpose is to investigate climate change impacts on water resources in the Loire River basin (around 110 000 km<sup>2</sup>), one of the main French river basins. Unlike the Seine and the Rhône river basins, the Loire River basin has not been yet extensively studied and no hydrological models of the entire basin currently exist. The ICC-HYDROQUAL project is, however, not limited to hydrological modelling. It also aims to evaluating the impacts on two related environmental aspects, the thermic regime and the biogeochemical quality of water streams. This two last points are of special interest in regard to the European Water Framework Directive, which commits member states to achieve good qualitative and quantitative status of all water bodies by 2015. Therefore, an integrated modelling framework has been proposed, inspired by the one of Ducharne et al. (2007). The project is organized in four complementary working packages:

1. Climate change impacts on water resources of the Loire River basin
2. Climate change impacts on the thermic regime of the Loire River and water streams
3. Climate change impacts on the biogeochemical quality of the Loire River and water streams
4. Vulnerability of the Loire River basin to climate change

## 1.3 Objectives of this thesis

The work presented in this thesis is part of the first working package of the ICC-HYDROQUAL project. One of the two hydrological models involved in this package is a catchment-based land surface model, the CLSM presented in Section 2.2. Prior to

---

<sup>1</sup><http://www.plan-loire.fr>

being driven by climate simulations to assess climate change impacts, a hydrological model must prove its ability to correctly capture the present time hydrological behavior of the studied basin. This step is fundamental to gain confidence in the reliability of future predictions. As previously mentioned, each step of an impact study introduces errors that propagate in the modelling chain with final model predictions that often contain large uncertainty. Limiting the errors at each step is therefore critical. As the uncertainties introduced by climate models are difficult to evaluate, a usual strategy is to consider an ensemble of projections. Concerning hydrological models, the uncertainty issue can be addressed through evaluation of present time performance and comparison between different models.

The main objective of this work lies in the calibration of the CLSM in the Loire River basin. Calibration is a critical step in the modelling process (see [Beven \(2001\)](#) for details). In a broad sense, it is an indirect process of model parameter estimation. Any computer-based model that intends to represent the behavior of a natural system conceptualizes the reality and introduces parameters to be specified. Generally, some parameters can be related to observations, but some others are not directly measurable or even cannot be assumed to have direct physical interpretations ([Gupta et al., 2005](#)). Therefore, the values of these parameters have to be adjusted to fit some observations. The estimation of parameters that results from the calibration step is theoretically only valid for the calibration period. To ensure that the model captures the overall behavior of the studied system, an independent evaluation of model performance is required. This step, called validation, aims at testing the extrapolation capacity of the model, given the chosen parameters. The reliability of further model simulations depends on the outcome of the validation step and the judgment of the modeller, regarding his objectives.

The work conducted during this thesis project includes, besides the calibration and validation of the CLSM, a critical analyze of the model behavior. Based on the results of the validation step, model sensitivity to two soil parameters is investigated. The soil depth and the wilting point are found to play a key role when facing drought events, which contributes to a better understanding of how the model reacts to extreme climatic conditions.

## 2 Model description

### 2.1 Land surface modelling

This section aims to briefly present the role of land surface models (LSMs) and how they have evolved from a simple approach representing the surface energy and water fluxes to more and more sophisticated and complex models. More details can be found in the reviews of [Pitman \(2003\)](#) and [Overgaard et al. \(2006\)](#). The former focuses on surface processes in climate models, while the latter presents a hydrological perspective.

#### 2.1.1 Background

Land surface models were introduced in atmospheric general circulation models (AGCMs) to simulate land surface energy and water fluxes, when provided with the relevant information on land surface and climate data. The two key equations that represent the role played by the surface are the surface energy balance and the surface water balance equations ([Pitman, 2003](#)).

**The surface energy balance:** The net radiation  $R_n$ , which is the net balance of the incoming  $S_{in}$  and reflected  $S_{out}$  shortwave radiation, and the incoming  $L_{in}$  and emitted  $L_{out}$  longwave radiation at the Earth's surface, is partitioned between sensible heat  $H$ , latent heat  $\lambda E$  and soil heat  $G$  fluxes:

$$R_n = S_{in} - S_{out} + L_{in} - L_{out} = H + \lambda E + G \quad (2.1)$$

**The surface water balance:** Precipitation at the surface  $P$  is partitioned between evaporation  $E$ , runoff  $Q$  and change in moisture storage  $\Delta S$ :

$$P = E + Q + \Delta S \quad (2.2)$$

Note that the two budgets are linked by the evaporation term and that any change in the energy balance affects the water balance. This link enhances the complexity of the interactions and feedbacks between atmospheric and land surface processes. For instance,  $H$  and  $\lambda E$ , which play a key role in the climate system, are sensitive to the albedo, roughness length and characteristics of plants (leaf area index, distribution of roots), but are also affected by the soil moisture available to plants to transpire.

### 2.1.2 Evolution of land surface models

According to the classification proposed by [Sellers et al. \(1997\)](#), the first-generation land surface models prescribed uniform surface parameters and used simple bulk aerodynamic transfer formulations to compute evaporation. This description of evaporation is related to the [Penman \(1948\)](#) approach, one of the earliest that considered the land surface as an electrical analogue. Using this approach, the “bucket” model by [Manabe \(1969\)](#) was the first scheme that explicitly represented hydrological processes. A single layer for soil moisture  $W$  was implemented, evaporation was proportionably limited by soil water content (when below a threshold  $W_k$ , smaller than the field capacity  $W_{FC}$ ) and runoff was generated if the soil moisture exceeded  $W_{FC}$ , globally fixed to 15 cm (Figure 2.1a).

Second-generation models appeared in the mid-80s. The new approach, commonly referred to as the soil-vegetation-atmosphere transfer (SVAT) approach, gives vegetation a more direct role in determining the surface energy and water balances, particularly by allowing stomatal conductance to decrease in response to increased environmental stress. Evaporation formulations were refined, usually based on a resistance diagram (illustrated in Figure 2.1b) inspired by the Penman-Monteith formulation ([Monteith, 1965](#)), and progressively evolved from the “big leaf” assumption to tile- or mosaic type of models and multi-layer models ([Overgaard et al., 2006](#)). Compared to the simple hydrology of the “bucket” scheme, second-generation schemes present large improvements in their representation of hydrological processes. For instance, complex soil moisture parameterizations were introduced and methods based on the [Richards \(1931\)](#) equation were implemented to represent the vertical transfer of water within the soil column (albeit usually in a simplified way).

[Koster et al. \(2000\)](#) reported that the SVAT models could be considered the “state of the art” according to a major international project, the Project for Intercomparison of Land surface Parametrizations Schemes (PILPS) ([Henderson-Sellers et al., 1993](#)). These models however strongly disagreed on how best to simulate land surface energy

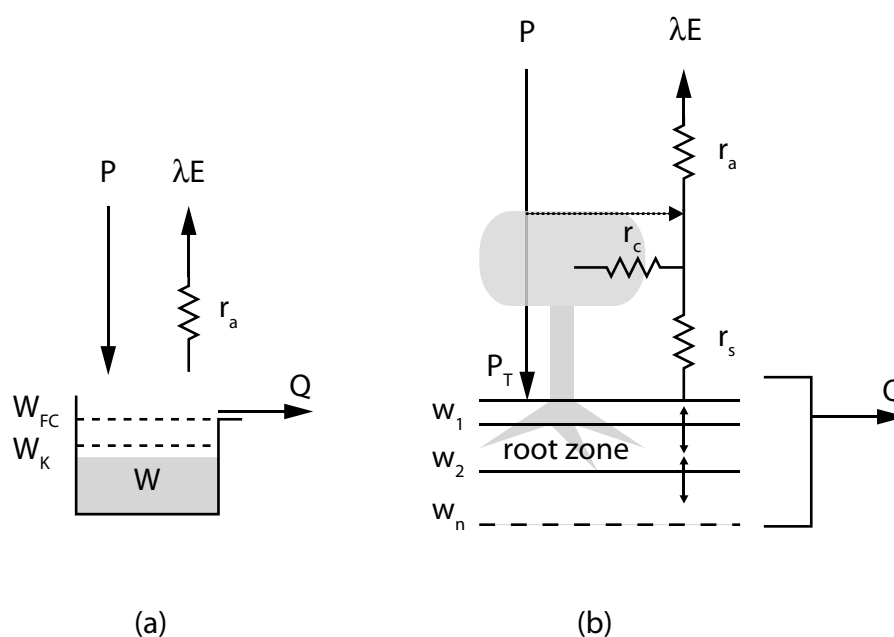


**Figure 2.1:** Illustration of (a) a first-generation land surface model and (b) a second-generation land surface model. Terms not defined in the text are  $P_T$  the through-fall,  $r_a$  the aerodynamic resistance,  $r_s$  the soil resistance and  $r_c$  the stomatal and/or canopy resistance. Reproduced from Gascoïn (2009).

and water fluxes. Investigating the wide disparity in the water balances generated by different PILPS schemes provided with the same information on the land surface and the same atmospheric forcing, Koster and Milly (1997) came to the conclusion that the runoff formulation controls evaporation rates as much as the evaporation formulation. Thus, several modelling groups have recognized the importance of better representing hydrological processes, whose parameterizations were still crude in comparison to sophisticated evaporation formulations. In particular, considering the one-dimensional nature of typical SVAT as a weakness to properly treat the runoff generation, Koster et al. (2000) presented a new strategy for modelling the surface component of the climate system. This led to the development of the Catchment Land Surface Model (CLSM) described in the next section.

## 2.2 The Catchment Land Surface Model (CLSM)

The CLSM was developed at the NASA Goddard Space Flight Center to improve the treatment of the subgrid horizontal structure of land surface hydrological processes, especially by explicitly accounting for subgrid soil moisture variability and its effects

on evaporation and runoff. The philosophy, the structure and the implementation of the CLSM are detailed in [Koster et al. \(2000\)](#) and [Ducharne et al. \(2000\)](#). A recent adaptation of the model, the version used in this study, can be found in [Gascoïn et al. \(2009\)](#). The presentation below is very strongly inspired by these articles and focuses on the main features that give the CLSM its originality.

The CLSM introduced two main innovations for modelling the land surface. First, the CLSM considers irregularly-shaped hydrologic catchments, with boundaries defined by topography, as the fundamental elements of the land surface instead of quasi-rectangular atmospheric grid elements<sup>1</sup>. Second, the CLSM uses the TOPMODEL framework ([Beven and Kirkby, 1979](#))<sup>2</sup> within each catchment to relate the subgrid soil moisture variability to characteristics of the topography. The distribution of soil moisture in the root zone allows the partitioning of the catchment into three hydrologically distinct regimes, wherein different regime-appropriate parameterizations are applied.

### 2.2.1 Soil moisture variability

The CLSM follows the pioneer work of [Famiglietti and Wood \(1994\)](#), who were the first to include the TOPMODEL formalism in a LSM, to relate the water table distribution to the topography. Thus, each catchment includes a water table defined under the same assumptions as in TOPMODEL:

1. The saturated hydraulic conductivity  $K_S$  decreases exponentially with depth  $z$  ( $z$  is positive underground):

$$K_S(z) = K_0 \exp(-\nu z) \quad (2.3)$$

where  $K_0$  is the saturated hydraulic conductivity at the soil surface and  $\nu$  characterises the decay of the saturated hydraulic conductivity with depth.

2. At all time steps, the water table distribution results from a steady-state under the uniform recharge rate of the time step.
3. The hydraulic gradients can be approximated by the topographic gradients.

---

<sup>1</sup>The CLSM can nevertheless use regular grid, as in two intercomparison projects: the Rhône-AGG project ([Boone et al., 2004](#)) and the recent ALMIP project ([Boone et al., 2009](#)).

<sup>2</sup>TOPMODEL is based on the concept of variable contributive area and accounts for the topographic influence on their distribution. Hence, it provides an objective way to parameterize first-order controls on water movement from topographic information.

Given these assumptions, the spatial distribution of the local water table  $z_D$  is related to the catchment mean water table depth  $\bar{z}$  by a simple relation:

$$z_D = \bar{z} - \frac{1}{\nu}(x - \bar{x}) \quad (2.4)$$

where  $x = \ln(a/\tan\beta)$  is the topographic index and  $\bar{x}$  the mean catchment value of the topographic index. The term  $a$  is the upslope contributing area per unit contour length and  $\tan\beta$  is the local topographic gradient.

This distribution is used to calculate the ‘‘catchment deficit’’  $M_D$ , a bulk variable defined as the average amount of water per unit area that would have to be added to saturate all of the catchment. Assuming that the unsaturated zone is initially in an hydrostatic equilibrium state, the form of the profile of soil moisture at an arbitrary point in the catchment, as derived from the relations of [Clapp and Hornberger \(1978\)](#), is:

$$\omega(z) = \left( \frac{\psi_S - z_D + z}{\psi_S} \right)^{-1/b} \quad (2.5)$$

where  $\omega$  is the degree of saturation (or ‘‘wetness’’) at the depth  $z$ ,  $\psi_S$  is the matrix potential in the soil at saturation and  $b$  is a soil parameter.  $M_D$  results from the three-dimensional integration of  $1 - \omega(z)$ , first vertically over the unsaturated zone (which gives the local moisture deficit) and then laterally over the catchment distribution of  $z_D$ . Thus, a given value of catchment deficit is associated with a unique description of equilibrium horizontal soil moisture variability. As this one-to-one theoretical relationship between  $M_D$  and  $\bar{z}$  cannot be written analytically, it is approximated in the CLSM with a simple analytical function ([Ducharne et al., 2000](#)).

Two additional bulk variables are introduced to account for non-equilibrium conditions. The ‘‘root zone excess’’  $M_{RZ}$  and the ‘‘surface excess’’  $M_{SE}$  describe the average amount of water per unit area by which the moisture, in the root zone and the top 2 cm respectively, differ from the value implied by the equilibrium profile (illustrated in [Figure 2.2](#)). The vertical water fluxes between the three bulk variables are computed at each time step based on the Richards equation and act to bring the system closer to equilibrium conditions.

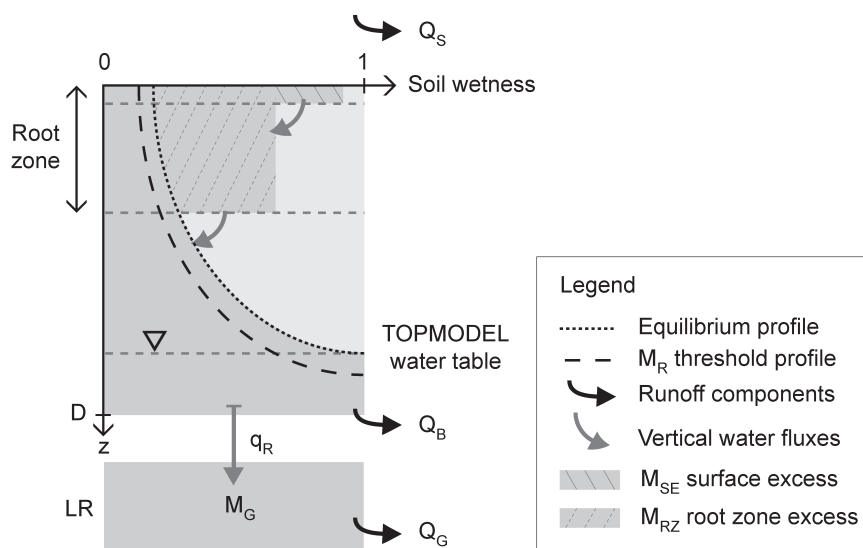


**Figure 2.2:** Vertical representation of soil moisture profile in the CLSM and water fluxes.  $z$  is the depth coordinate and  $D$  the total depth of the soil layer connected with the surface.  $M_D$  corresponds to the area above the equilibrium profile. Note that  $M_{SE}$  and  $M_{RZ}$  are positive, illustrating the case of a storm. Reproduced from Gascoïn et al. (2009).

## 2.2.2 Spatial partitioning within the catchment

The three bulk moisture variables allow the catchment to be separated into three distinct regions: the “saturated” region, the “transpiration” region and the “wilting” region. Each region is characterized by a root zone moisture status, respectively saturated, intermediate and stressed (the root zone moisture lies below the vegetation-specific wilting point  $\omega_{wilt}$ ). The areal fractions are determined through manipulation of a probability density function (pdf) of root zone soil moisture. The “equilibrium” pdf of root zone soil moisture is first derived from the pdf of water table depth and then corrected by using  $M_{RZ}$  to account for non-equilibrium conditions (Figure 2.3). In practice, the three fractions vary according to the values of  $M_D$  and  $M_{RZ}$  through several manipulations and approximations (Ducharne et al., 2000). Note that when the water table depth lies below the assumed bedrock depth (depth of the soil layer connected with the surface), i.e. when  $M_D$  exceeds a threshold value  $M_D^B$ , the determination of the “equilibrium” pdf is revised because no free-standing water table is assumed to exist anymore in the catchment. By default,  $M_D^B$  is defined as the catchment deficit corresponding to the soil depth.

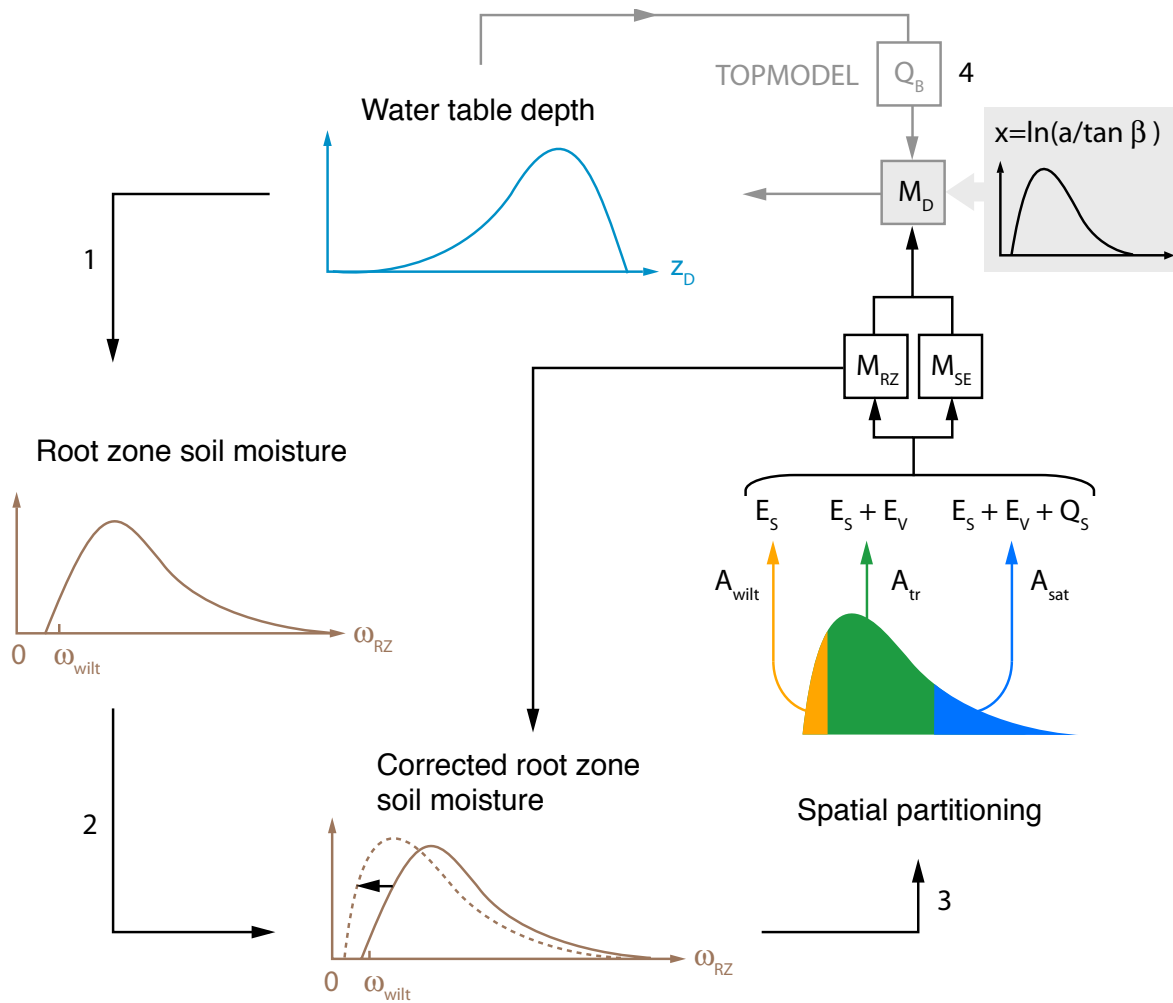


**Figure 2.3:** Schematic representation of CLSM spatial partitioning process. Terms not defined in the text are  $E_S$  the bare soil evaporation and  $E_V$  the transpiration. Note that to simplify the schema, the pdf of root zone soil moisture is not correctly represented. The area corresponding to  $A_{sat}$  should be represented by a Dirac function. Reproduced from Gascoïn (2009).

### 2.2.3 Energy and water budgets

The CLSM is continually partitioning each catchment into three subregions, wherein the physical mechanisms that control evaporation and runoff generation are fundamentally different. This explicit separation allows one to employ the appropriate treatments in each.

**Energy budget:** The energy balance calculations, mostly taken from the Mosaic LSM of [Koster and Suarez \(1996\)](#), are adapted to each subregion. The resistances applied to the evapotranspiration calculation vary significantly between the subregions. Resistance to bare soil evaporation is a function of surface soil moisture and is therefore small in the saturated fraction, moderate in the transpiration fraction and high in the wilting fraction. In the wilting fraction, the canopy resistance is set high enough to shut down transpiration completely, while it is a function of vegetation type, solar radiation and ambient air temperature but moisture stress in the two other regions.

**Water budget:** The total runoff  $Q$  simulated by the CLSM is, in its original version, the sum of two components: the surface runoff  $Q_S$  and the subsurface downslope flow  $Q_B$  (TOPMODEL's baseflow).

The throughfall  $P_T$  falls uniformly on all three catchment subregions. The CLSM uses the concept of variable contributing area, here given by the saturated fraction  $A_{sat}$ , to estimate the saturation-excess overland flow:

$$Q_S = P_T A_{sat} \quad (2.6)$$

The infiltration-excess overland flow is also described in the CLSM. It depends on the surface excess moisture:

$$P_T - Q_S > M_{SE}^{max} - M_{SE} \Rightarrow Q_S = P_T - (M_{SE}^{max} - M_{SE}) \quad (2.7)$$

where  $M_{SE}^{max}$  is the maximum possible surface excess, given the soil moisture in the top soil layer and the soil properties.

The TOPMODEL framework ([Sivapalan et al., 1987](#)) relates baseflow, here the subsurface flow, to the mean water table  $\bar{z}$ :

$$Q_B = \frac{K_0}{\nu} \exp(-\bar{x} - \nu \bar{z}) \quad (2.8)$$

where  $K_0$  is the saturated hydraulic conductivity at the soil surface. Note that, according to the use of an active soil depth in the calculation of the areal fractions, the baseflow is shut off when the catchment deficit exceeds the threshold value  $M_D^B$ .

The subsurface flow described above is limited by TOPMODEL's framework, which only represents a shallow water table with hydraulic gradients parallel to the surface. Such a conceptual water table is not comparable to deep multi-layered aquifer systems and is in particular not adapted to store water over long timescales. To account for groundwater storage in a deep aquifer, [Gascoïn et al. \(2009\)](#) introduced an additional term  $Q_G$  in the runoff formulation. The deep component  $Q_G$  is generated from an additional linear reservoir LR, which has no spatial variability and is recharged by the flux  $q_R$  when the catchment deficit is below a threshold  $M_G$  (Figure 2.2):

$$M_D < M_G \Rightarrow q_R = (M_G - M_D)dt/\tau_R \quad (2.9)$$

where  $\tau_R$  is the timescale that controls the rate of recharge when it occurs. The threshold  $M_G$  is lower than  $M_D^B$  and can be defined as:

$$M_G = \alpha M_D^B \quad (2.10)$$

where  $\alpha$  is a calibration parameter. The outflow from the reservoir is computed for each time step  $dt$  using a linear storage-discharge relationship:

$$Q_G = S_G \frac{dt}{\tau_G} \quad (2.11)$$

where  $S_G$  is the amount of water into the reservoir and  $\tau_G$  is the timescale that controls the groundwater discharge. Typically, the timescale  $\tau_G$  should have values between a few tens of days up to a couple of years.

The implementation of the resulting scheme contributes to a better representation of water transfers. It particularly led to considerable improvement in the simulated runoff of the groundwater driven catchment of the Somme River (France), where the original runoff formulation was not adapted ([Gascoïn et al., 2009](#)).

## 2.2.4 Validation and applications

The interest of the CLSM has been originally demonstrated in the Red-Arkansas River Basin (566 251 km<sup>2</sup>, United States) (Ducharne et al., 2000). The model was then evaluated in two international projects, the PILPS Phase 2(e) experiment (Nijssen et al., 2003) and the Rhône-AGG project (Boone et al., 2004). Most of the applications of the CLSM focus on the modelling and assimilation of soil moisture (see Reichle et al. (2008) for a recent example), now integrated within the Land Information System (LIS) framework<sup>3</sup> (Kumar et al., 2008). Among other recent applications, Mahanama et al. (2008) investigated the role of soil moisture initialization in streamflow prediction in Sri Lanka, and Wang et al. (2009) used the CLSM and other state-of-the-art LSMs to reconstruct drought over the United States.

In France, the CLSM has been used to assess climate change impact on hydrology in the Seine River basin (Ducharne et al., 2007). It has also been the main modelling tool of Gascoïn (2009), who applied the CLSM in very contrasted regions. He especially focused on hydrological parameterizations of the model and showed the importance of properly representing processes at various scales, from topsoil to aquifers.

Since the first “bucket model”, the representation of hydrological processes in LSMs has been considerably improved. Particularly, the catchment-based approach of the CLSM and the partitioning within each catchment theoretically allow more realistic calculations of the water budget. The CLSM makes use of topographic information to compute surface runoff, groundwater and subgrid distribution of soil moisture. Thus, the CLSM can be used as a stand-alone hydrological model. Moreover, the physical basis of this energy-based LSM makes it an attractive alternative to the more conceptual type of evapotranspiration models traditionally applied in hydrological modelling.

---

<sup>3</sup><http://lis.gsfc.nasa.gov/>

## 3 Modelling the Loire River basin

The purpose is to develop a robust and satisfactory application of the CLSM in the Loire River basin, based on historical data. It is a fundamental step to gain confidence in the modelling framework before modelling impacts of future changes. To do so requires input data and validation data. This work has been carried out during a preliminary phase of the ICC-HDROQUAL project ([Bustillo, 2008](#)).

### 3.1 Study site and data description

#### 3.1.1 The Loire River basin

The Loire River, with 1010 km, is the longest river in France. From its source in the Ardèche at about 1370 m above sea level, it flows north then west through the Massif Central to the Atlantic Ocean (Figure [3.1](#)). Its watershed, which covers one fifth of France (about 120 000 km<sup>2</sup>), is characterized by varying climate and lithology (see Appendix [A.1](#)). The Loire is subject to heavy flooding and important seasonal fluctuations in volume. Spring floods alternate with dry summers causing very low water levels.

#### 3.1.2 Data sources

The Loire watershed upstream Montjean, which is the outlet of the basin considered in this study, was subdivided into 68 unit catchments, with an average size of about 2000 km<sup>2</sup> (Figure [3.2](#)). Each catchment is a computational unit for the CLSM, so that the modelling can be considered as semi-distributed. Catchment delineation was based on a 50-m resolution digital elevation model (DEM). Particular attention was given to



Figure 3.1: Map of the Loire basin. Source: GRID-Europe

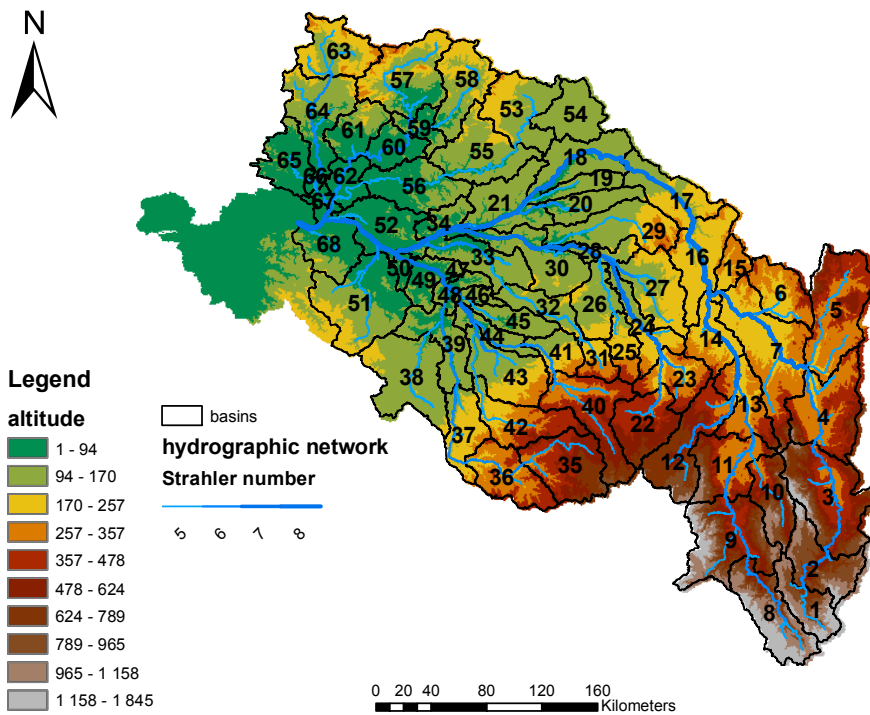


Figure 3.2: Delineation of the 68 unit catchments in the Loire River Basin.

define unit catchments that can be regarded as homogeneous (regarding the vegetation and geological characteristics) and whose outlets are located at or near gauging stations.

Topographic index computation in each unit catchment was based on the same DEM. The topographic index distribution is approximated by a three-parameter gamma function (Sivapalan et al., 1987; Ducharne et al., 2000).

As a classical LSM, the CLSM takes as input near-surface meteorological variables (rainfall, snowfall, shortwave and longwave incident radiation, surface pressure, air temperature and humidity at 2 m, wind speed at 10 m). The atmospheric forcing data are provided hourly, at 8-km resolution, by the SAFRAN analysis system. The analysis combines large-scale fields from an operational weather prediction model and ground observations from the networks of Météo-France through optimal interpolation. A detailed description and assessment of the SAFRAN analysis over France is presented by Quintana-Segui et al. (2008). For the CLSM, the 8-km SAFRAN data were aggregated by weighted means to each unit catchment.

The vegetation and soil parameters were derived from the ECOCLIMAP database (Masson et al., 2003). Intended to initialize SVAT schemes, it provides a complete surface parameter dataset at 1-km resolution. Each grid cell is described by a vegetation class (among 215) with associated root zone and soil depth and morphological characteristics given at the monthly time scale (leaf area index, vegetation fraction, roughness length, emissivity and albedo). For the CLSM, the vegetation classes from ECOCLIMAP are translated to the 8 classes defined by the Mosaic LSM. Concerning soil parameters, percentages of clay, silt and sand allow to define in each 1-km grid cell a soil texture class using the USDA textural triangle. Hydraulic parameters (saturated hydraulic conductivity for compacted soil  $K_{SC}$ , soil matrix potential at saturation  $\psi_S$ , b parameter from Clapp and Hornberger (1978)) are then deduced for each class from Cosby et al. (1984). Vegetation and soil parameters are aggregated by arithmetic means to each unit catchment.

Finally, observed daily streamflow data are obtained from the Banque Hydro website (<http://www.hydro.eaufrance.fr>). Gauging stations are mostly located at or near the outlet of the unit catchments (Figure 3.3) and are assumed to provide good quality data. However, discharge series are sometime incomplete and others are known to be influenced by human activities (industry, agriculture) and water management (several dams are used for flood protection and low flow mitigation). Due to lack of information, these anthropogenic influences are not taken into account in the simulations.

## 3.2 Modelling results

### 3.2.1 Calibration strategy

The calibration strategy presented here follows the one that was previously applied in the Seine and Somme river basins (Ducharne et al., 2009a; Gascoin et al., 2009). For each catchment, the calibration is performed by comparing the observed discharge at the outlet and the total runoff simulated by CLSM over the upstream catchments. Since no routing procedure is included in the CLSM<sup>1</sup>, 10-day averages are used to compare discharge and runoff. This time step is assumed to be larger than the concentration time of the entire basin, what allows to neglect the routing issue. The calibration is conducted recursively and progressively from upstream catchments to downstream catchments. Once a parameter set is chosen for an upstream catchment, the runoff simulated in this catchment is considered fixed when calibrating downstream catchments. Thus, each catchment is characterized by only one parameter set. For ungauged catchments, the calibration is performed by evaluating simulations at the nearest downstream catchment. In those cases, the simulations use the same parameter set for both catchments.

In each gauged unit catchment, the quality of the simulation is assessed using two objective functions. The relative bias in total runoff ( $\%BiasR$ ) focuses on the long-term water balance:

$$\%BiasR = \frac{\sum_t(Qsim_t - Qobs_t)}{\sum_t(Qobs_t)} \times 100 \quad (3.1)$$

where  $Qsim_t$  and  $Qobs_t$  denote the simulated and the observed flow respectively, at the instant  $t$ . The Nash-Sutcliffe ( $NS$ ) efficiency is used to evaluate the goodness of fit of the model:

$$NS = 1 - \frac{\sum_i(Qobs_i - Qsim_i)^2}{\sum_i(Qobs_i - \bar{Qobs}_i)^2} \quad (3.2)$$

where  $Qsim_i$  and  $Qobs_i$  denote here the 10-day average of the simulated and observed flow respectively.

Although the two objective functions help to select an “optimal” parameter set for each catchment, the method differs from optimization in at least two points. First,

---

<sup>1</sup>A routing scheme based on the Muskingum method has been implemented for the Seine River basin but it has not been yet adapted to the Loire River basin.

the parameters are arbitrarily chosen, based on knowledge and expertise gained from previous applications and literature review. The resulting parameter combinations that can be tested are fixed a priori. Second, a visual inspection of the simulated hydrograph is performed for each catchment. The choice of the “optimal” parameter set results from a subjective trade-off between the statistical performances ( $\%BiasR$  and  $NS$ ) and the visual inspection.

Parameter	Units	Value									
$K_{mult}$	-	1	10	100							
$\nu$	$m^{-1}$	1	2	3	4						
$\alpha$	-	0.1	0.2	0.3	0.4	0.5	0.6	0.7	0.8	0.9	1
$\tau_G$	days	91	182	365	730						

**Table 3.1:** Parameter values tested for the CLSM-LR.

Four parameters have been calibrated. Two are linked to the TOPMODEL’s framework and characterize the exponential profile of the saturated hydraulic conductivity  $K_S$ : its value at the soil surface  $K_0$  and the parameter  $\nu$  describing its vertical decay (equation (2.3)). The two others,  $\tau_G$  and  $\alpha$ , control the groundwater linear reservoir (equation (2.11)) and its recharge (equation (2.10)). The a priori values of the parameters are given in Table 3.1. Note that  $K_0$  is calibrated via a multiplicative coefficient  $K_{mult}$ , starting from the default value deduced from ECOCLIMAP, which exhibits spatial variations following the variability in soil texture. Thus, 480 parameter combinations describe the parameter space for each unit catchment<sup>2</sup>. Besides, 12 parameter combinations using only the values of  $K_{mult}$  and  $\nu$  are used to determine parameter sets specific to the CLSM version without LR. Two versions can be compared: one using only these 12 parameter combinations (CLSM without LR) and the other using the 492 possible combinations (CLSM with or without LR). Finally, an “optimal” parameter set with constant values over the entire basin has been selected for each version of the CLSM. This enables to compare a “lumped” calibration (when the goodness to fit is only assessed at the outlet of the basin) and a “distributed” calibration (when all catchments are progressively calibrated). Hence four parameter sets have been selected.

The simulation period is 1976–2007. Each simulation is initialized by a 5-years spin-up time. Following a split-sample methodology, the remaining period is divided into a

<sup>2</sup>The number of combination is of course constraint by computational resources. Running a 15-years simulation, associated to one parameter set, takes almost one hour on a personal computer.

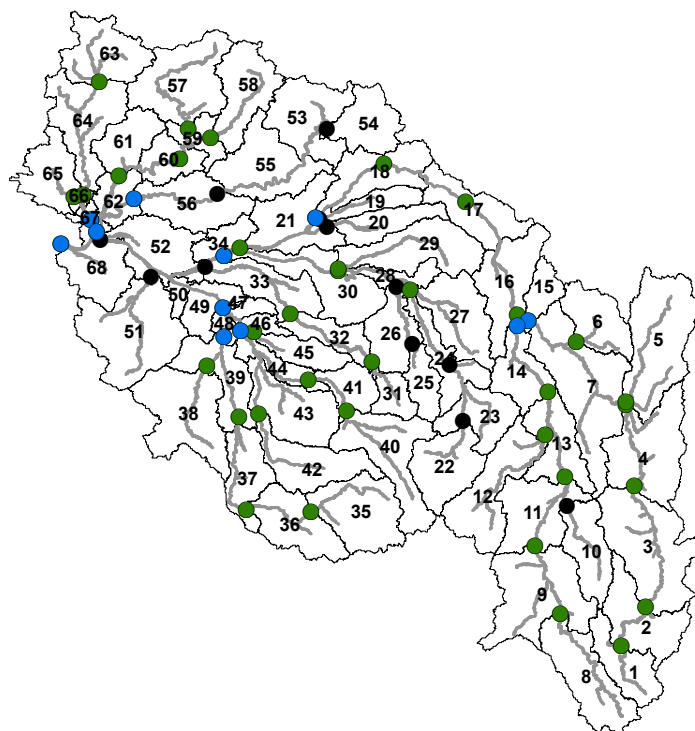


**Figure 3.3:** Location of the 58 gauging stations. Green dots: 46 stations selected for the analysis of results. Blue dots: 11 stations selected to reflect the hydrological behavior of the Loire River and its main tributaries.

calibration period, from August 1976 to July 1992, and a validation period, from August 1992 to July 2007.

### 3.2.2 Analysis of results

The selected parameter sets are presented in Appendix A.2 (Table A.2). The corresponding simulations are denoted by Nor4 and R4on to distinguish between the two version of the CLSM previously mentioned. Nor4 refers to the CLSM without LR, while R4on refers to the CLSM with or without LR. The simulation denoted by Nor4.g2.k2 corresponds to the one chosen though the “lumped” calibration process: the combination of  $\nu = 2$  and  $K_{mult} = 10$  is chosen as the “optimal” parameter set for the CLSM without LR, when considering constant values over the entire basin. It is also found better than any combinations using constant values of the LR parameterization, suggesting that the LR parameterization does not yield better results if not calibrated in each unit catchment. This outcome differs from the results of the calibration conducted in the Seine River Basin (A. Ducharne, personal communication).

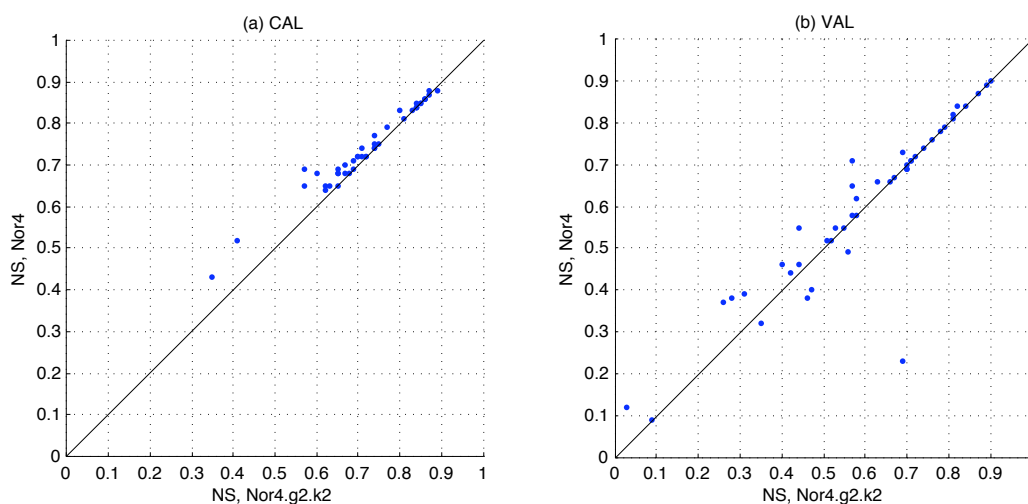


**Figure 3.4:** Scatter plots of efficiency for the Nor4.g2.k2 and the Nor4 simulations: CAL=calibration period, VAL=validation period. Note that in (a) and (b) two points are located outside the plotting range because of negative  $NS$  values.

The following analyses use the results at 46 selected gauging stations (Figure 3.3). Only stations where more than 5 years of discharge data are available in both the calibration and the validation periods are retained.<sup>3</sup>

First, the overall performance of the Nor4.g2.k2 and the Nor4 simulations are compared. In terms of efficiency, the Nor4 simulation is better than the Nor4.g2.k2 one (Figure 3.4). Its  $NS$  values are higher in almost all stations during the calibration period. The validation period, despite more contrasted results, confirms the global improvement offered by the distributed version. In terms of water balance, the two simulations do not present significant difference (not shown). Consequently, the “distributed” calibration globally improves the performance of the CLSM compared to the “lumped” one. Note, however, that they do not largely differ. The difference between positive  $NS$  values in both periods does not exceed 0.12. Moreover, no difference can be visually detected on the simulated hydrographs at the outlet of the basin (where the “lumped” calibration has been performed), which is coherent with obtaining very similar  $NS$  and  $\%BiasR$  values at this station (Table 3.2). Therefore, the Nor4.g2.k2 simulation can be considered as a good approximation of the Nor4 one. This shows that for the CLSM without LR, the parameter set chosen globally allows to capture the overall behavior of the basin almost as well as the “distributed” parameter set.

<sup>3</sup>Additionally, two unit catchments (n°23 and n°54) are excluded because of significant difference between catchment and associated gauging station drainage areas (see Table A.1).

	Mean $Q_{obs}$ ( $\text{m}^3 \text{s}^{-1}$ )	Mean $Q_{sim}$ ( $\text{m}^3 \text{s}^{-1}$ )	$\%BiasR$	$NS$
<i>Calibration period</i>				
Nor4.g2.k2	961	1062	10.56	0.74
Nor4	961	1076	11.96	0.74
R4on	961	1070	11.32	0.77
<i>Validation period</i>				
Nor4.g2.k2	870	1052	20.85	0.57
Nor4	870	1070	22.97	0.58
R4on	870	1060	21.81	0.64

**Table 3.2:** Statistical performances at the basin outlet (Loire at Montjean, catchment n°68) for both the calibration period (1976–1992) and the validation period (1992–2007).

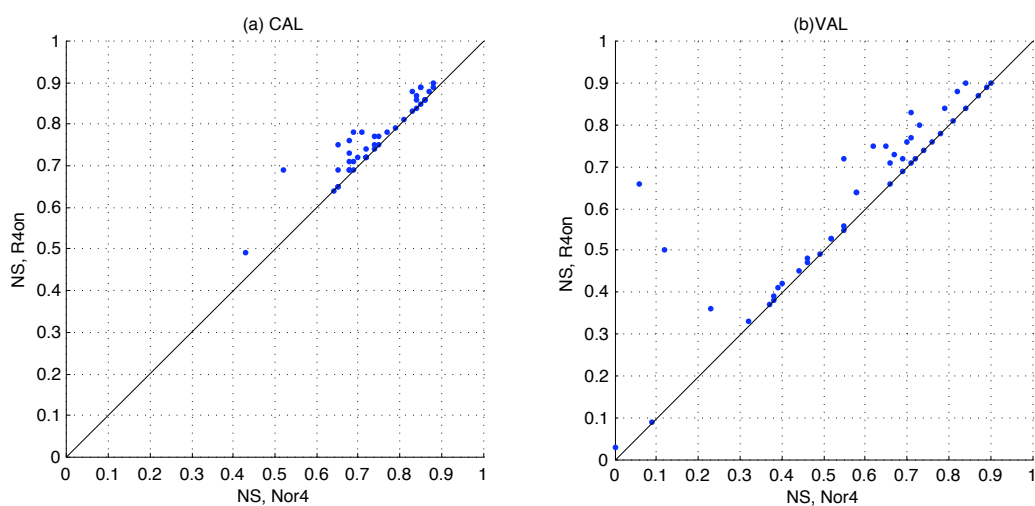


**Figure 3.5:** Scatter plots of efficiency for the Nor4 and the R4on simulations: CAL=calibration period, VAL=validation period. Note that in (a) two points are located outside the plotting range because of negative NS values.

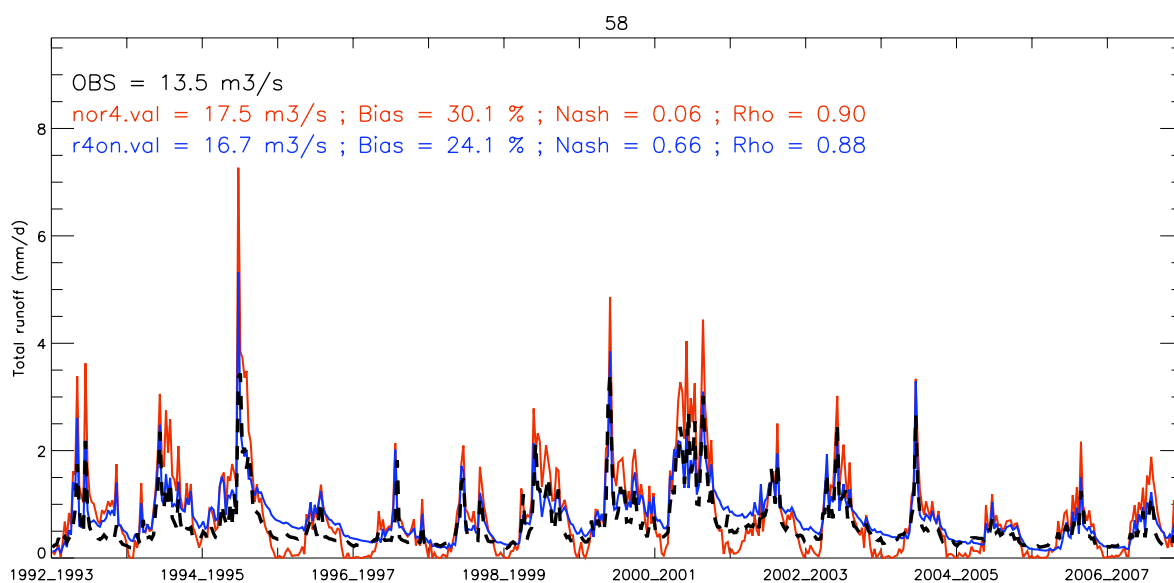


**Figure 3.6:** Comparison between observed and simulated discharges (10-day averages in mm/d) at the outlet of the catchment n°58 during the validation period (from August 1992 to July 2007).

The overall performance of the distributed Nor4 and the R4on simulations are compared in Figure 3.5. In terms of efficiency, the R4on simulation performs better than the Nor4 one, with systematically higher  $NS$  values during both periods. This clearly shows that the LR parameterization yields better performances. Remarkably,  $NS$  values at two stations increase by more than 0.35 during the validation period. The simulation of the runoff in one of these stations (outlet of the catchment n° 58) illustrates particularly well how the additional reservoir LR (equation (2.11)) improves the simulation. This upstream catchment is geologically characterized by sandstones and marls. The calibrated parameters,  $\alpha = 0.7$  and  $\tau_G = 365$  days, indicate that an important role is given to the linear reservoir. Figure 3.6 compares the total runoff from the two simulations. Similarly to the results presented in Gascoin et al. (2009), the linear reservoir allows long term storage and thus smoothes the simulated runoff. High flows are reduced and low flow are sustained.

A scatter plot of  $NS$  values (Figure 3.7) between the calibration and validation periods is used to report the overall efficiency of the R4on simulation, which is considered the best available simulation given the chosen calibration strategy. As expected, the efficiency deteriorates when going from the calibration to the validation period. Among the 46 gauging stations, 35 stations have an efficiency that can be considered as “fair” ( $NS > 0.7$ ) during the calibration period, while 23 stations have such efficiency during

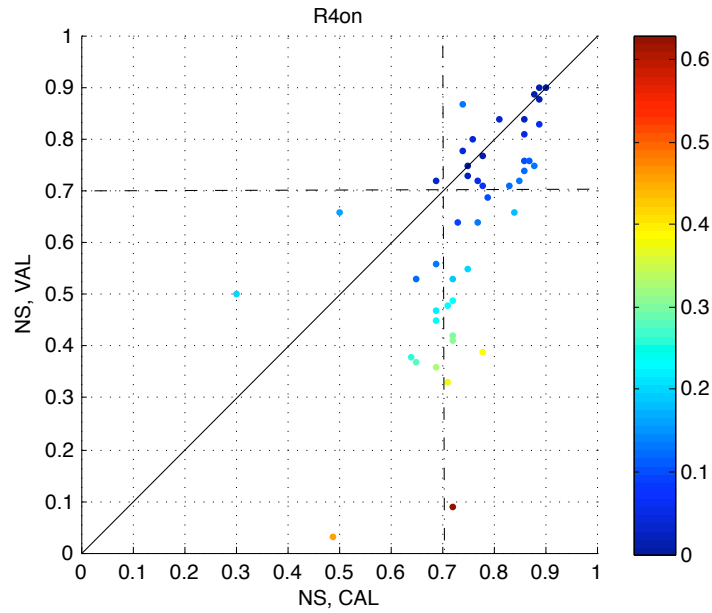


**Figure 3.7:** Scatter plot of efficiency for the R4on simulation: CAL=calibration period, VAL=validation period. The colormap indicates the absolute difference of *NS* values between calibration and validation periods.

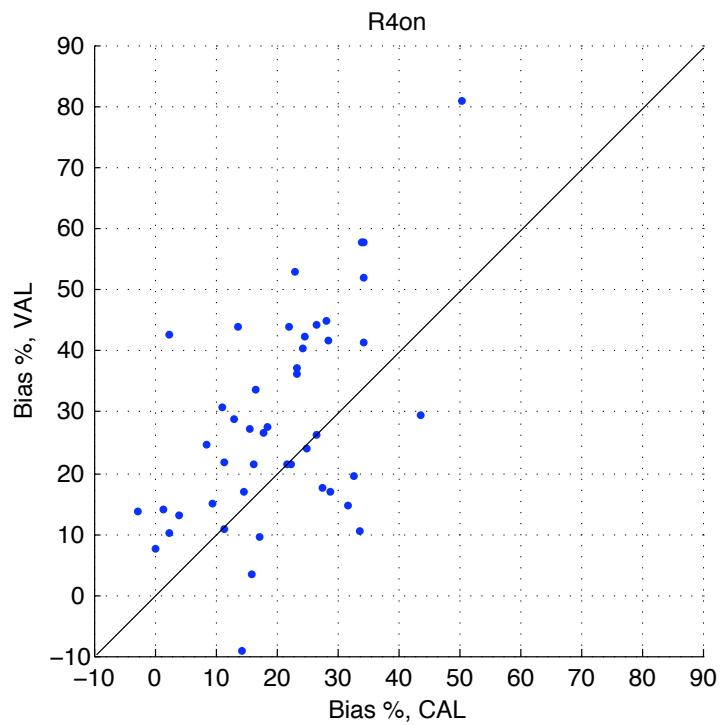


**Figure 3.8:** Scatter plot of relative bias in total runoff for the R4on simulation: CAL=calibration period, VAL=validation period.

the validation period. The median  $NS$  value decreases from 0.75 to 0.70 when moving from calibration to validation period. As shown on Figure 3.8, there is a strong tendency to overestimate annual simulated discharges in both calibration and validation periods. The median  $\%BiasR$  value increases from 21.81% to 26.41% when moving from calibration to validation period.

According to these results, it seems that the R4on simulation does not perfectly capture the hydrological behavior of a majority of catchments.

Nevertheless, the overall behavior of the Loire River basin seems reasonably represented. Table 3.3 presents the results obtained at the outlets of large sub-basins. 11 stations were selected to reflect the hydrological behavior of the Loire River and its main tributaries (Figure 3.3). During the validation period, only one station performs poorly ( $NS < 0.5$ ), 2 have efficiency that can be considered as reasonable ( $0.5 \leq NS < 0.6$ ), 3 as “rather good” ( $0.6 \leq NS < 0.7$ ) and 5 as “fair” ( $NS \geq 0.7$ ). Besides, the seasonal and interannual variability of the observed discharge at the outlet of the river basin is well simulated, as shown on Figure 3.9 for the validation period. In term of water balance, the performances are more limited. The relative bias in total runoff is within 20% for all but 2 stations during the calibration period, but generally increases during the validation period.

Unit catchment	River	Location	Area (km <sup>2</sup> )	$\%BiasR$		$NS$	
				CAL	VAL	CAL	VAL
7	Loire	Nevers	17 570	12.75	28.73	0.79	0.69
14	Allier	Cuffy	14 310	13.60	44.15	0.78	0.39
18	Loire	Blois	38 320	18.36	27.48	0.69	0.56
30	Cher	Savonnières	13 680	8.41	24.79	0.73	0.64
39	Vienne	Ingrandes	10 050	0.02	7.59	0.90	0.90
44	Creuse	Leugny	8 020	16.02	21.47	0.86	0.84
48	Vienne	Nouâtre	19 920	11.16	10.81	0.89	0.88
56	Loir	Durtal	7 925	43.51	29.39	0.30	0.50
66	Mayenne	Montreuil-Juigné	5 803	17.21	9.51	0.89	0.90
67	Maine	Angers	22 020	28.60	16.79	0.76	0.80
68	Loire	Montjean	109 930	11.32	21.81	0.77	0.64

**Table 3.3:** Performance of the R4on simulation at 11 selected stations: CAL=calibration period, VAL=validation period.

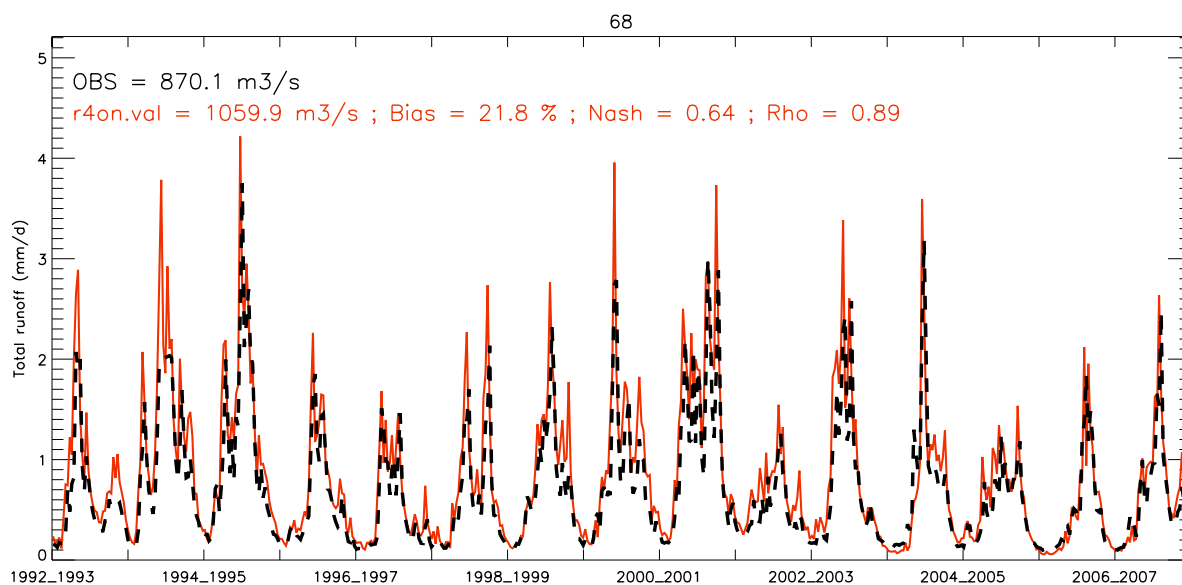


**Figure 3.9:** Comparison between observed and simulated discharges (10-day averages in mm/d) of the Loire River at Montjean (outlet of the basin) during the validation period (from August 1992 to July 2007).

Note that the analysis of the results is limited by the lack of information about anthropogenic influences. Large reservoirs in the upstream part of the river basin are used to prevent floods and mitigate summer low flows. Agriculture and industries also influence river flows, especially in the middle part of the river basin. In particular, water consumption may have increased significantly between the calibration and the validation periods, which may partly explains why the relative bias in total runoff globally increases when moving to the latter period.

## 3.3 Sensitivity analysis

### 3.3.1 Motivation

The main objective of an independent validation is to determine whether or not the simulation and its associated set of parameters can be considered as acceptable and reliable given the modelling objective. As the purpose of the ICC-HYDROQUAL project is to assess hydrological impacts of climate change, a strong tendency to overestimate annual discharges can be considered as a subject worthy of further investigation. In particular, for the three selected simulations, the bias at the outlet of the basin exceeds 20% during

the validation period, while it is close to 10% during the calibration period (Table 3.2). A large relative bias in total runoff can be explained by several factors, including errors in the forcing data (especially errors in precipitation), errors in the observation of the river flow, missing processes (e.g. groundwater leaks), or water withdrawals. In this study, all these errors are difficult to quantify.

The following is based on the assumption that the total evaporation is globally underestimated and that this assumed underestimation is exacerbated when moving from the calibration to the validation period. This is only an attempt to better understand the model behavior and its sensitivity to some parameters. Note, however, that in-depth analysis of a sophisticated land surface model is a considerable task, and that finding a solution to possible model flaws is not in the scope of this master's thesis project.

In the CLSM, the evaporation parameterization results from a complex interaction between the energy balance calculations derived from the Mosaic LSM and the spatial partitioning into three subregions (Section 2.2). In particular, the model is assumed to achieve a smooth transition between the full transpiration and full wilting regimes through the dynamically varying areas of the subregions (Koster et al., 2000). Hence, the wilting fraction plays a key role in the energy and water budgets.

Unlike previous applications of the CLSM in the Seine and the Somme river basins (Ducharne et al., 2007, 2009a; Gascoïn et al., 2009), but as it has been done in Koster et al. (2000); Boone et al. (2004, 2009), the soil depth and the wilting point have not been calibrated in this study. The default values in each unit catchment are here derived from the ECOCLIMAP dataset.

To study the influence of the soil depth and the wilting point in the Loire River basin, sensitivity to these two soil parameters is investigated. Particular attention is given to the influence of these two parameters on the dynamic of the wilting fraction, also called the stressed fraction.

### 3.3.2 Sensitivity to the soil depth

The sensitivity to soil depth is investigated by doubling the default soil depth values in the Nor4.g2.k2 simulation, hereafter called DEF. The resulting simulation is denoted Z2. Table 3.4 gives simple statistical measures of the spatial distribution of soil depth values. As shown in Figure 3.10, the stressed fraction associated to Z2 is negligible compared to the one of DEF. The transpiration is consequently not limited by water

stress during summer periods, which explains the increase in total evaporation (despite the decrease in bare soil evaporation). An overall decrease in total runoff is observed. It can be related to the decrease in baseflow (the surface runoff being almost similar in both simulations) and seems coherent with the large increase in catchment deficit (i.e. reduction in catchment moisture). This increase of catchment deficit may be attributed to the increase in summer transpiration and root-uptake. The comparison shows that the stressed fraction, controlling the “moisture-stressed” evaporation regime, almost vanishes when the soil depth is doubled and that the impact on the resulting water and energy budgets is not negligible (Table 3.5). This outcome implies that the soil depth plays a key role in determining the stressed fraction.

	<i>Soil depth (m)</i>			
	Min	Max	Mean	Std.dev
DEF	1.88	2.61	2.13	0.13
Z2	3.76	5.22	4.26	0.25

**Table 3.4:** Statistics of the soil depth values. Std.dev: standard deviation.

Variable	Units	DEF	Z2	Relative variation (%)
Precipitation rate	mm/yr	858	858	
Total runoff	mm/yr	303	267	-12
Total evaporation	mm/yr	550	581	6
Stressed fraction	%	8.2	1.0	-88
Catchment deficit	mm	134	236	76

**Table 3.5:** Annual averages of some variables simulated by the DEF and the Z2 simulations over the Loire River basin during the validation period.

As presented in Section 2.2, the soil depth does not directly influence the partitioning process, but it plays an indirect role, because it controls the range of the catchment deficit. The soil depth is used to derive two threshold values,  $M_D^B$  and  $M_D^{max}$ .  $M_D^B$ , as already mentioned, is defined as the catchment deficit corresponding to the soil depth, while  $M_D^{max}$  is the maximum value of  $M_D$ , imposed to eliminate an unrealistic drift in the moisture state variables during extended dry periods (Koster et al., 2000). When the catchment deficit  $M_D$  exceeds  $M_D^B$ , the associated water table depth lies below the soil depth, which is used as a proxy for the bedrock depth. In such a case, hereafter called the

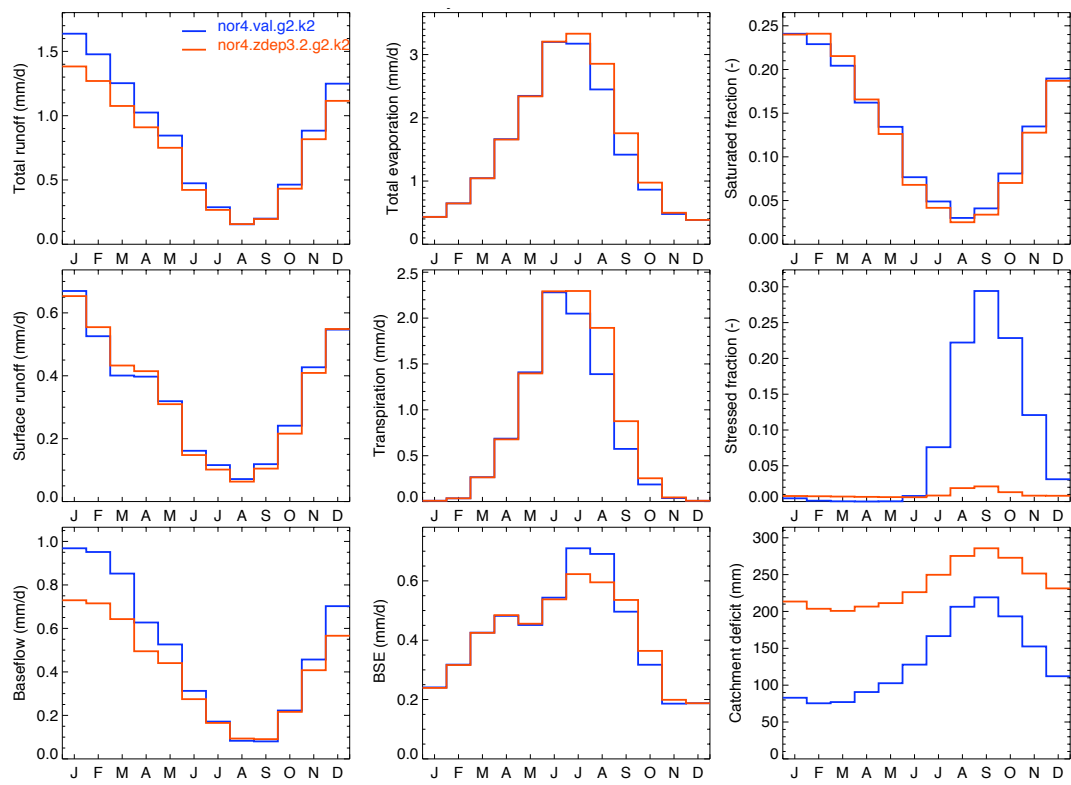


**Figure 3.10:** Comparison of some hydrological variables from DEF (nor4.val.g2.k2, blue line) and Z2 (nor4.zdep3.2.g2.k2, red line) (annual cycle averaged over the validation period and over the entire basin). BSE: bare soil evaporation.

“no water table” case, the TOPMODEL framework cannot be used anymore, because no-free standing water table is assumed to exist in the catchment, and the partitioning process is revised. This is done by using a ramping procedure between the two threshold values  $M_D^B$  and  $M_D^{max}$ . Because the ramping procedure aims at reducing effectively the catchment deficit,  $M_D^{max}$  has to be close from  $M_D^B$ . By default,  $M_D^{max}$  is calculated as the catchment deficit at one meter below the soil depth.

	$M_D^B$ (mm)				$M_D^{max}$ (mm)			
	Min	Max	Mean	Std.dev	Min	Max	Mean	Std.dev
DEF	130.58	405.63	197.67	57.04	239.42	629.88	344.85	87.21
Z2	381.40	1094.52	563.73	156.79	563.52	1447.09	798.32	205.05

**Table 3.6:** Statistics of the thresholds values  $M_D$  and  $M_D^{max}$ . Std.dev: standard deviation.

In the DEF simulation (when using the soil depth and the wilting point values given by the ECOCLIMAP database), the “no water table” case is found to entirely control the stressed fraction. In each unit catchment, the stressed fraction only occurs when the catchment deficit  $M_D$  exceeds  $M_D^B$  (Figure 3.11) and is then calculated by the above ramping. The differences stated between the two simulations DEF and Z2 are mainly related to this threshold behavior. In the Z2 simulation, the two threshold values  $M_D^B$  and  $M_D^{max}$  significantly increase (Table 3.6), and in the majority of unit catchments, the “no water table” case is never reached (situation 1: Z2 in Figure 3.11). In these catchments (where  $M_D < M_D^B$ ), there are either no stressed fraction, or stressed fractions that seldom occur. Note that in these catchments, the stressed fraction is associated with the partitioning process controlled by the wilting point, as described in Section 2.2. In the other unit catchments, the “no water table” case occur despite large threshold values.

An example of the behavior associated with the “no water table” case in the Z2 simulation is displayed in Figure 3.12. Before 1989, the catchment deficit  $M_D$  of the Z2 simulation follows the one of the DEF simulation, despite the fact that no stressed fraction is simulated in the Z2 simulation, whereas a stressed fraction is simulated almost each summer in the DEF simulation, following the treatment of the “no water table” case described above. During the extended dry period 1989–1990, however, the Z2 catchment deficit strongly diverges from the DEF one. While the catchment deficit is reduced in DEF thanks to the ramping procedure of the “no water table case”, the Z2 catchment deficit largely increases. This difference is linked to the absence of a stressed fraction in

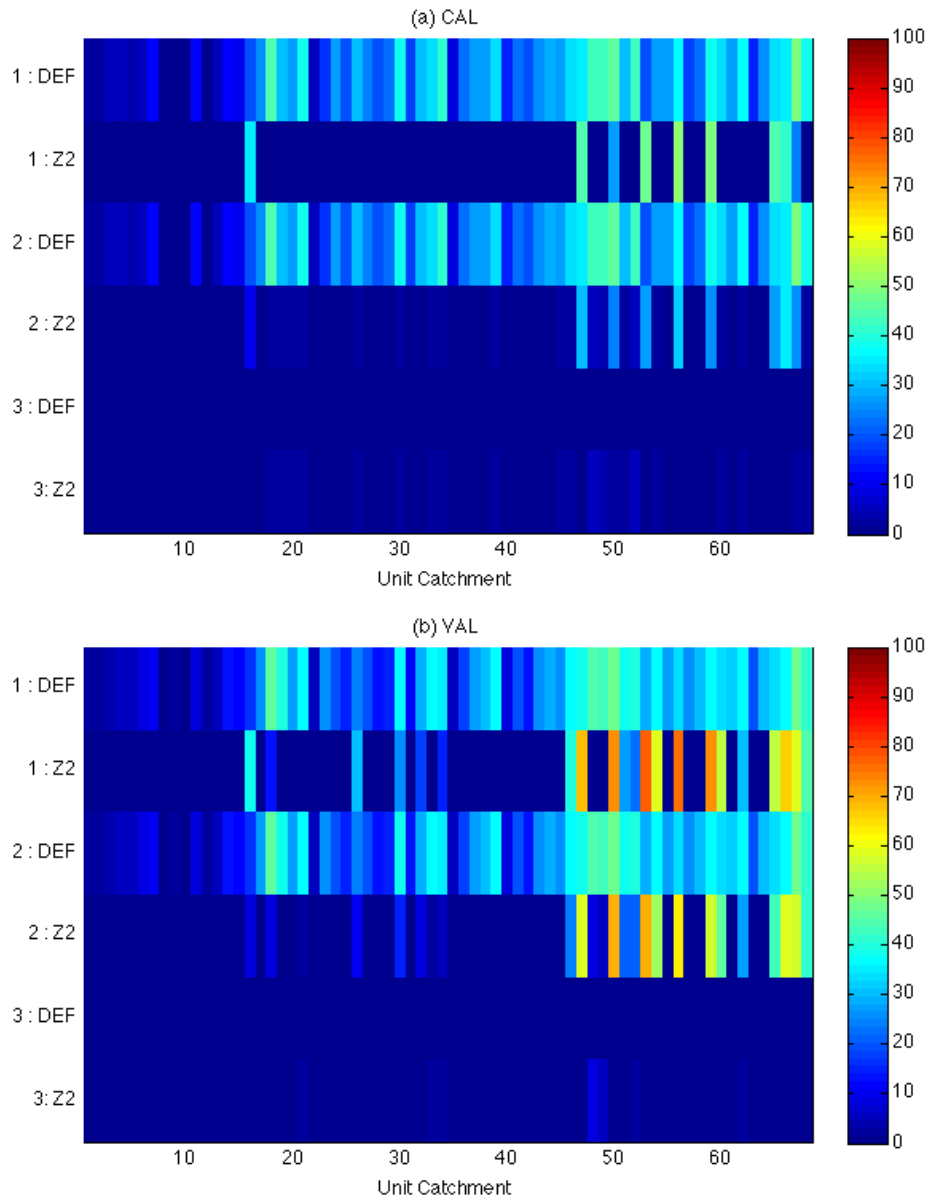


**Figure 3.11:** Comparison in the 68 unit catchments, between the DEF and the Z2 simulations, of the occurrences, in terms of frequency, of three following situations:  
 1:  $M_D > M_D^B$   
 2:  $ar4 > 0$ , where  $ar4$  denotes the stressed fraction  
 3:  $ar4 > 0$  and  $M_D < M_D^B$   
 CAL=calibration period, VAL=validation period.

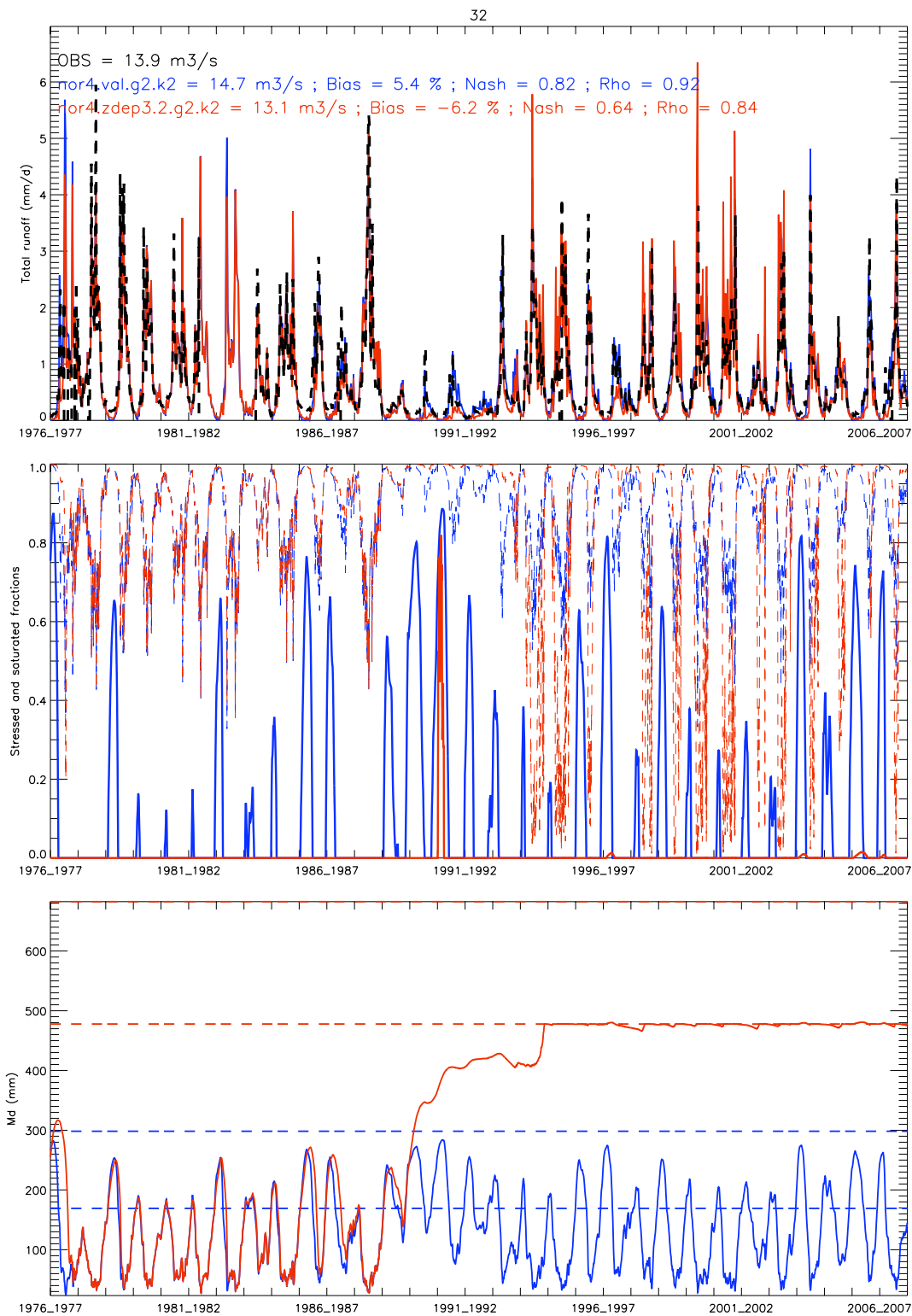


**Figure 3.12:** Top, comparison between observed and simulated total runoff (10-day averages) from DEF (nor4.val.g2.k2, blue line) and Z2 (nor4.zdep3.2.g2.k2, red line) at the outlet of the unit catchment n°32 (the total runoff is the sum of the runoff simulated in the unit catchments n°31 and n°32). Note the strong reduction (simulated and observed) of runoff during the period 1989–1991. Middle, comparison between the stressed fractions simulated by DEF and Z2 (the saturated fractions are also displayed, with an inverted axis). Bottom, comparison between the catchment deficits of both simulations.

the Z2 simulation, what leads to unstressed transpiration and large moisture depletion during the dry period. In this unit catchment, the stressed fraction only appears when the catchment deficit has already diverged, and the catchment deficit does not recover from the dry period and seems stuck once he reaches the threshold  $M_D^B$ . In such a situation, there is no interaction anymore between the equilibrium water table and the root zone excess  $M_{RZ}$  (Section 2.2), as indicated by the very small vertical water fluxes between the two bulk moisture variables  $M_D$  and  $M_{RZ}$  (not shown). This behavior is probably linked to the formulation or the parameterization of the transfer of moisture between  $M_D$  and  $M_{RZ}$  (details in Koster et al. (2000); Ducharne et al. (2000)). In particular, the timescale used in this formulation is related to  $M_D$  and  $M_{RZ}$  by an empirical function. In essence, this timescale decreases with decreasing  $M_D$  and with increasing  $M_{RZ}$ . It may be possible that the exponential form of this empirical function, whose effectiveness is shown in Ducharne et al. (2000), is not adapted to the range of values of  $M_D$  and  $M_{RZ}$  that can be found in the present case.

In the unit catchment presented here and in all the unit catchments where  $M_D$  reaches  $M_D^B$  in the Z2 simulation, the divergence of the catchment deficit compared to the one simulated by the DEF simulation, and the inability of the model to recover, seem to result from the combination of an absence of a stressed fraction when facing particularly strong drought event and the absence of interaction between the water table and the root zone afterward. Note that in other unit catchments, the Z2 catchment deficit may also diverge from the DEF one for the same reason (absence of a stressed fraction), but in these catchments the model do recover from the drought event.

The main issue highlighted by the comparison between the DEF and Z2 simulations is that the “moisture-stressed” evaporation regime, which is associated with the stressed fraction, almost vanishes when doubling the default soil depth values (Figure 3.10 and Table 3.5), because the partitioning process does not seem to effectively produce a stressed fraction outside the “no water table case”.

In the partitioning process of the CLSM, the wilting point plays a key role, because it divides the wilting subregions, where transpiration is turned off, from the two others subregions, where transpiration occurs with no water stress (Section 2.2). The results of the comparison presented above suggest that the wilting point derived from the ECO-CLIMAP database is too small to be effective. This point is investigated by a brief analysis of the sensitivity to the wilting point.

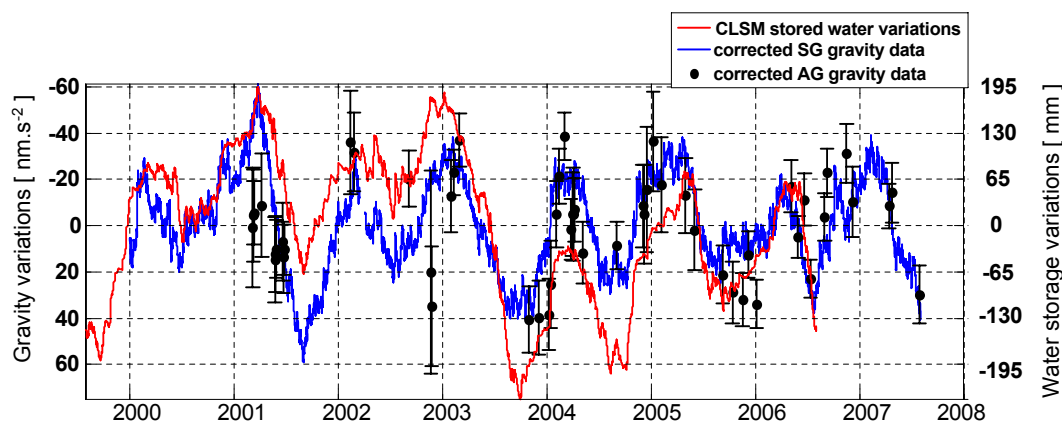


**Figure 3.13:** Comparison between modeled and observed gravity variations. The modeled variations are deduced from the variation of stored water simulated by the CLSM and the observed variations (using the superconducting gravimeter SG and absolute gravimeters AG) are corrected from atmospheric and global hydrological contributions. Reproduced from [Longuevergne et al. \(2009\)](#).

### 3.3.3 Sensitivity to the wilting point

The wilting point is expected to influence the simulated evaporation. Increasing the value of the wilting point should increase the stressed fraction, reduce transpiration, and thus reduce total evaporation.

The sensitivity of the CLSM to the wilting point parameter has been recently addressed by [Longuevergne et al. \(2009\)](#). Superconducting gravimeter monitoring was used to validate the water budget simulated by the CLSM at the scale of several hundreds of meters. The study is particularly interesting because it allows comparing simulated water storage to observations. [Longuevergne et al. \(2009\)](#) state that the gravity variation deduced from stored water variations simulated by the CLSM is in good agreement with observed gravity variations (Figure 3.13). The seasonal signal is well simulated and most of short-term variations are described. However, they point out significant errors during both summers 2001 and 2003. In 2001, the depletion is underestimated, whereas it is overestimated in 2003. The authors, assuming that the overestimated moisture depletion during the 2003 summer heat wave is mostly linked to modeled evapotranspiration, investigated the sensitivity to the wilting point. They showed that the agreement between the CLSM and observations can be significantly improved by considering a high wilting point value (0.75 instead of the default value 0.37, in degree of saturation). They also identified a wilting point threshold, as changing the wilting point from 0.37 to 0.60 does not change significantly the modelling results.

The results presented in [Longuevergne et al. \(2009\)](#) indicate that much higher values of the wilting point than the default one are needed to effectively reduce the overestimated moisture depletion simulated during the 2003 summer. This implies that the wilting point must be set high enough to effectively produce a stressed fraction and thus limit transpiration and moisture depletion during a dry period.

	pF	$\omega_{wilt}$			
		Min	Max	Mean	Std.dev
DEF	4	0.25	0.49	0.37	0.05
Z2	4	0.25	0.49	0.37	0.05
Z2.pF3	3	0.41	0.65	0.55	0.06
Z2.pF2.5	2.5	0.52	0.76	0.66	0.06

**Table 3.7:** Statistics of the wilting point values. The wilting point  $\omega_{wilt}$  is expressed in degree of saturation. Std.dev: standard deviation.

The sensitivity to the wilting point is investigated in the Loire River basin by comparing four simulations. In addition to the DEF and Z2 simulations already mentioned, two simulations with higher wilting point values are used. By default, the wilting point is chosen to be the soil moisture value, in degree of saturation, when the soil water potential  $\psi$  drops to -100 m. According to [Musy and Soutter \(1991\)](#), this corresponds to a temporary wilting point. The wilting point is calculated in each unit catchment from soil parameters deduced from [Cosby et al. \(1984\)](#), based on the soil texture classes derived from the ECOCLIMAP database. A convenient way to characterize the wilting point is to use the log transform of the water potential  $\psi$ , expressed in cm:  $pF = \log_{10}(-\psi)$ . Characteristics of the four simulations are given in Table 3.7. The Z2.pF3 and Z2.pF2.5 simulations only differ from the Z2 simulation by their definition of the wilting point.

Compared to the Z2 simulation, the higher values of the wilting point in the Z2.pF3 and Z2.pF2.5 simulations induce larger stressed fractions (Figure 3.14 and Table 3.8). The moisture stress is more effective, as indicated by the decrease in transpiration and total evaporation in summer, and the global decrease of catchment deficit. Total runoff increases with increasing wilting point, what is linked to the increase in baseflow and decrease in catchment deficit. Besides, increasing the wilting point seems to bridge the gap between the Z2 simulation and the DEF simulation, as indicated by comparable overall behavior (Figure 3.14). The DEF simulation and the Z2.pF2.5 simulation are not supposed to provide similar results, as they largely differ in their soil parameterization

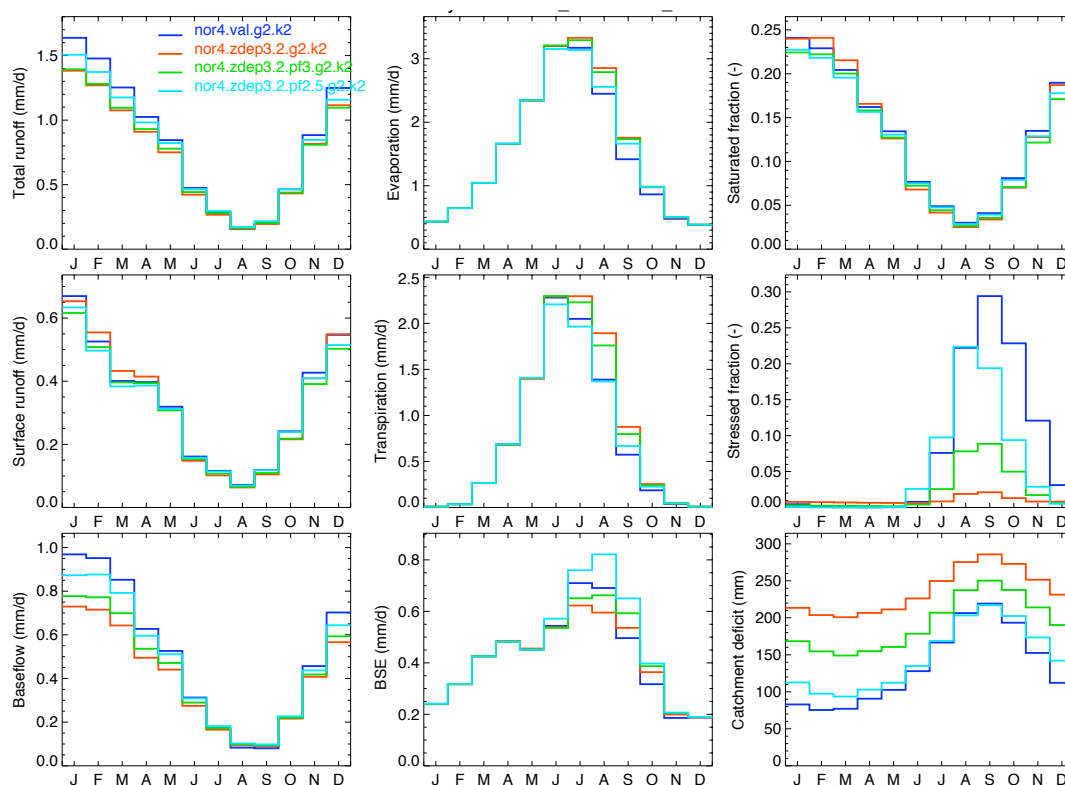


**Figure 3.14:** Comparison of some hydrological variables from DEF (blue line), Z2 (red line), Z2.pF3 (green line) and Z2.pF2.5 (cyan line) (annual cycle averaged over the validation period and over the entire basin). BSE: bare soil evaporation.

(soil and wilting point values), but the convergence suggest that comparable behaviors in the overall basin can be simulated by different ways. The stressed fraction is indeed controlled by the “no water table” case in the DEF simulation, while it mainly results from the effectiveness of the wilting point in the Z2.pF2.5.

Variable	Units	DEF	Z2	Z2.pF3	Z2.pF2.5
Precipitation rate	mm/yr	858	858	858	858
Total runoff	mm/yr	303	267	271	288
Total evaporation	mm/yr	550	581	579	563
Stressed fraction	%	8.2	1.0	2.3	5.6
Catchment deficit	mm	134	236	192	147

**Table 3.8:** Annual averages of some variables simulated by the DEF, Z2, Z2.pF3 and Z2.pF2.5 simulations over the Loire River basin during the validation period.

As presented in Section 3.3.2, the catchment deficit of Z2, in some unit catchments, largely increases during the dry spell of 1989–1990 until it reaches the threshold  $M_D^B$ . Figure 3.15 shows the influence of the wilting point on this behavior in the same unit catchment as in Figure 3.12. The catchment deficits of Z2, Z2.pF3 and Z2.pF2.5 diverge from the one of DEF during the dry period, but the divergence is more limited in the Z2.pF3 and Z2.pF2.5 simulations. Moreover, the catchment deficits of these two simulations slowly recover, whereas the one of the Z2 simulation does not. The limitation of the catchment deficit seems to be linked to the occurrence and the magnitude of the stressed fraction. In particular, the difference between the fractions simulated by the Z2 and the Z2.pF3 simulations during the dry period (Figure 3.15, bottom) enables the model to recover.

This example suggests that high wilting point values permit an effective soil moisture control on evaporation, and help preventing large moisture depletion during severe droughts. However, as already stated for the Z2 simulation, each unit catchment faces differently climatic conditions, and the value of the wilting point that would be necessary to avoid large increase of catchment deficit is probably specific to each unit catchment facing a particular drought event. A question that arises is whether the calibration process should or could take this issue into consideration. But it should also be kept in mind that the wilting point interacts with other parameters that influence the model behavior. For instance, the behaviors shown in Figure 3.12 for the Z2, Z2.pF3 and Z2.pF2.5 simulations depend of course of the soil depth value, as it controls the threshold  $M_D$  that defines the “no water table” case. In particular, the observed increases of catchment deficit could certainly be mitigated by a wise combination of the soil depth and wilting point values.

### 3.3.4 Discussion

The sensitivity analysis presented above was motivated by the assumption that the overall overestimation of annual discharges observed in the Loire River basin was linked to an underestimation of total evaporation. At this point, it should be acknowledged that no clear explanation has been provided, but the above sensitivity analysis highlighted some interesting points, which could contribute to a better understanding of how the CLSM simulates the soil moisture control on evaporation.

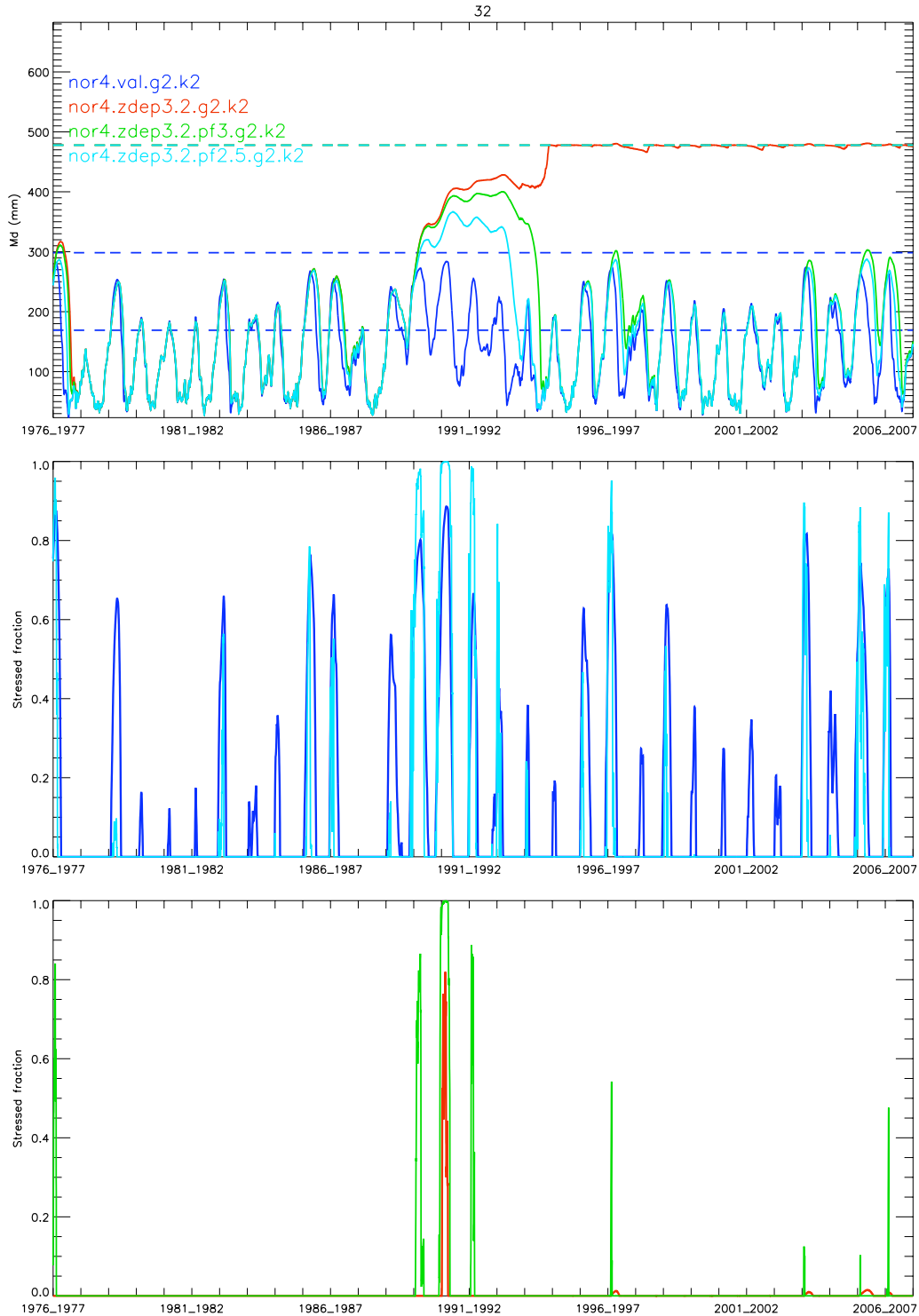


**Figure 3.15:** Top, comparison between the catchment deficits of DEF (blue line), Z2 (red line), Z2.pF3 (green line) and Z2.pF2.5 (cyan line) in the catchment n°32. Middle, comparison between the stressed fractions simulated by DEF and Z2.pF2.5. Bottom, comparison between the stressed fractions simulated by Z2 and Z2.pF3.

First, the soil depth is shown to play a key role in Nor4.g2.k2<sup>4</sup>. When using default soil depth and wilting point values, the stressed fraction is linked to the position of the catchment deficit compared to two threshold values derived from the soil depth. When the catchment deficit  $M_D$  exceeds the threshold value  $M_D^B$ , which is defined as the catchment deficit at the soil depth, the water table cannot follow TOPMODEL's distribution and a ramping procedure is used to treat this threshold situation. This ramping procedure is very effective to constrain the catchment deficit and to avoid a drift in the moisture state variables during extended dry periods, as revealed by the comparison with simulation Z2. This effectiveness in reducing  $M_D$  when it exceeds  $M_D^B$  is mainly due to the limitation of the outgoing water fluxes. In particular, the baseflow is shut off and the stressed fraction increases to restrict transpiration. This implies that the soil depth, if considered as a calibration parameter, could be used to influence the presence of the threshold situation and the effectiveness of its associated ramping procedure.

Next, the default value of the wilting point is shown to be too small to induce an effective soil moisture control on evaporation. A recent application of the CLSM presented in Longuevergne et al. (2009) also pointed out this issue, which seems crucial in the case of extreme warm weather situations. Using higher values increases the stress fraction and thus reduces transpiration. The wilting point could thus be used, if considered as a calibration parameter, to influence the effectiveness of the model to react to dry climatic conditions.

The main question that arises from the work presented in this section is then whether the two parameters should be calibrated. Wise combinations of these two parameters certainly offer the opportunity to simulate soil moisture control on evaporation by combining the role of the wilting point and the effectiveness of the threshold behavior associated with the soil depth. But adding degrees of freedom to the calibration is not necessarily good, especially when the data available for the calibration are limited, as in this study, where the only sources of observed data are river discharge. It is likely that a large number of widely different parameter sets could yield identical results with respect to objective functions based on river discharge. The problem of non-uniqueness, or indeterminacy, more commonly known as the equifinality problem (e.g., Beven and Binley, 1992; Beven and Freer, 2001), could be difficult (but not impossible) to overcome. In this sense, further work would be required to study the interaction between parame-

---

<sup>4</sup>The same conclusions can be drawn for the two others calibrated simulations (not shown).

ters (including the four parameters already calibrated in this study), and to develop a calibration strategy that could deal with such complexity.

# 4 Conclusion

## 4.1 Summary

This work was realized within the framework of the ICC-HDROQUAL project, the main purpose of which is to investigate climate change impacts on water resources in the Loire River basin. In particular, the first working package of the ICC-HYDROQUAL aims at assessing the potential effects of climate change impacts on the hydrological regime of this basin. In this work, which benefited from the model set-up carried out during a preliminary phase of the project, a catchment-based land surface model, the CLSM, was calibrated through a manual strategy, based on historical data of observed river discharges. The main purpose was to obtain a satisfactory application of the CLSM in the Loire River basin, a fundamental step to establish reliability of future model projections. To ensure that the model correctly captures the overall behavior of the basin, an independent evaluation of model performance was conducted, following the classical split-sample method. The overall behavior of the Loire River basin is found to be reasonably represented. In particular, the seasonal and interannual variability of the observed discharge at the outlet of the basin is well simulated. Nevertheless, an overall tendency to overestimate annual discharges has motivated further investigation. A sensitivity analysis of the model to two soil parameters, the soil depth and the wilting point, was conducted and several interesting points were highlighted, which could contribute to a better understanding of how the CLSM simulates the soil moisture control on evaporation. The main questions that arise are first, whether these two parameters should be included in the calibration process, and then, if they should, how to deal with the higher degree of complexity resulting from the introduction of new parameters in the calibration process. These are challenging questions, and further work is required to go deeper into these issues.

## 4.2 Perspectives

The calibration process is in fact even more challenging when the purpose of the modelling is, as in this project, to study the impact of climate change. The independent validation does not necessarily guarantee that the calibrated model will be able to cope with different climatic conditions. The recent application of the CLSM in the Seine River basin illustrates the difficulties that can arise when assessing climate change impacts. In the framework of the RExHySS project, the comparison between different state-of-the-art hydrological models (including parsimonious lumped model, semi-distributed model and distributed model) has shown that the CLSM, despite comparable results during the validation period, differs from the other models in its response to climate change. The CLSM showed an increase in evaporation, leading to a stronger reduction of total runoff under future conditions than the other models (Ducharne et al., 2009b). This behavior has been judged unrealistic, based on the results from Longuevergne et al. (2009). Possible explanations for such a behavior have been proposed, including the role of the wilting point (which could not be sufficiently effective), the role of the effective soil depth (which controls the storage capacity), and the importance of the connection between the conceptual water table (which follows TOPMODEL's framework) and the surface, what allows to sustain transpiration through root-uptake. However, no clear solution has been given until now, partly because the sophistication of the model, where multiple simulated processes are involved and interact in a complex way, does not facilitate its full understanding.

The simulations calibrated during this project will be used to assess climate change impacts in the Loire River basin (the model being driven by several climate forcings), and the results will be compared to those of the other model involved in the ICC-HYDROQUAL project. The insights provided by Longuevergne et al. (2009) and the sensitivity analysis presented here might then help to analyze the results of the CLSM. In this sense, investigating the sensitivity of the model to the soil depth and the wilting point under climate change could be particularly interesting, because it would allow one to study the influence of calibrating the soil depth and the wilting point on the model response to climate change.

Parameterizations of hydrological processes in land surface and climate modelling are of crucial importance to properly represent water and energy fluxes (e.g., Gascoïn, 2009). In particular, soil parameterization and its associated representation of water movement in soil strongly influence the complex interplay between energy and water at

the land surface, because they influence the dynamics of evapotranspiration, runoff and soil moisture. Importance of soil moisture (especially through soil moisture memory) in the land-atmosphere interactions has been highlighted in several studies (e.g., [Koster et al., 2004](#)), and is expected to play an increasing role in future climate change, particularly in Europe ([Seneviratne et al., 2006](#)). In this sense, the way land surface and climate models represent this coupling is crucial. For instance, [Boe and Terray \(2008\)](#) linked the changes in evapotranspiration over France and central Europe in the CMIP3 models<sup>1</sup> to the different ways these climate models represent the respective role of soil moisture and radiative energy at surface on evapotranspiration in the present climate, with consequences on simulated changes in temperature and precipitation. A better representation of the land-atmosphere interactions, including the controls on evapotranspiration, could certainly contribute to more realistic climate projections. In particular, this is the starting point of a Ph.D. project, the purpose of which is to improve future climate projections of a regional climate model by investigating the representation of soil water fluxes dynamic. The CLSM and another state-of-the-art land surface model, ORCHIDEE ([Krinner et al., 2005](#)), will first be evaluated off-line by comparison with soil moisture data and surface flux measurements, what should provide new insights into the behavior of the models and could lead to a better representation of soil water fluxes.

---

<sup>1</sup>These models were used in the phase 3 of the Coupled Model Intercomparison Project, in the context of the IPCC AR4.

# A Appendices

## A.1 Study site and characteristics of the unit catchments

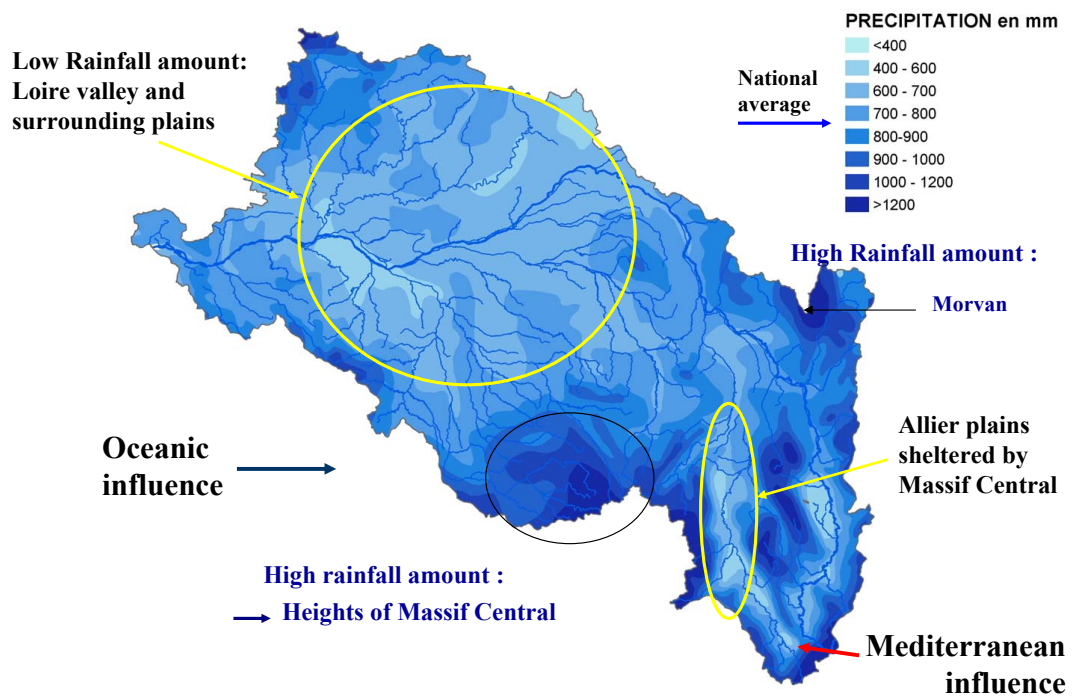


Figure A.1: Mean annual precipitation. Source: V. Bustillo

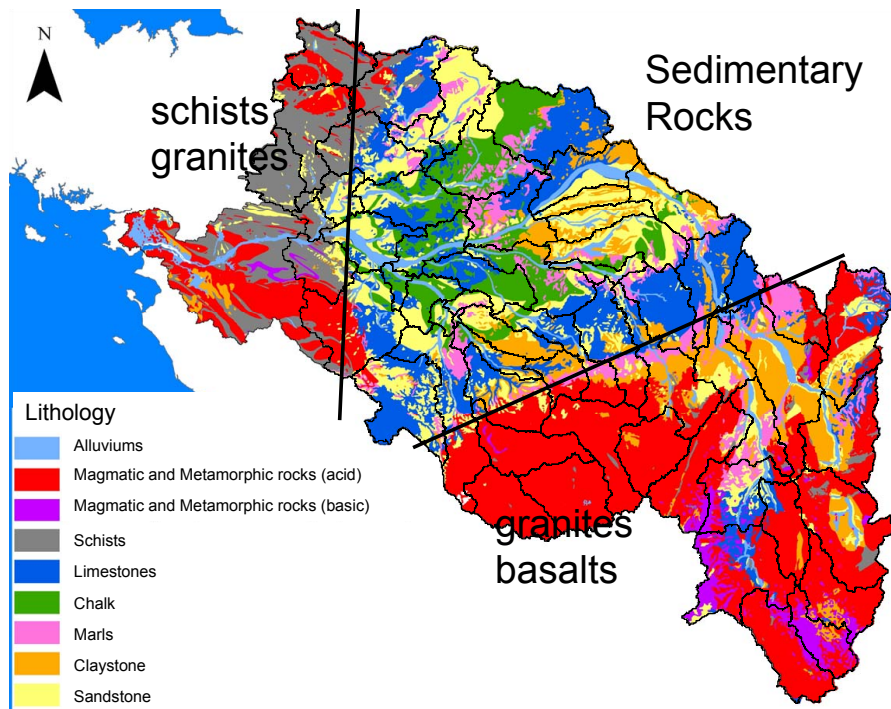


Figure A.2: Map of lithology. Source: V. Bustillo

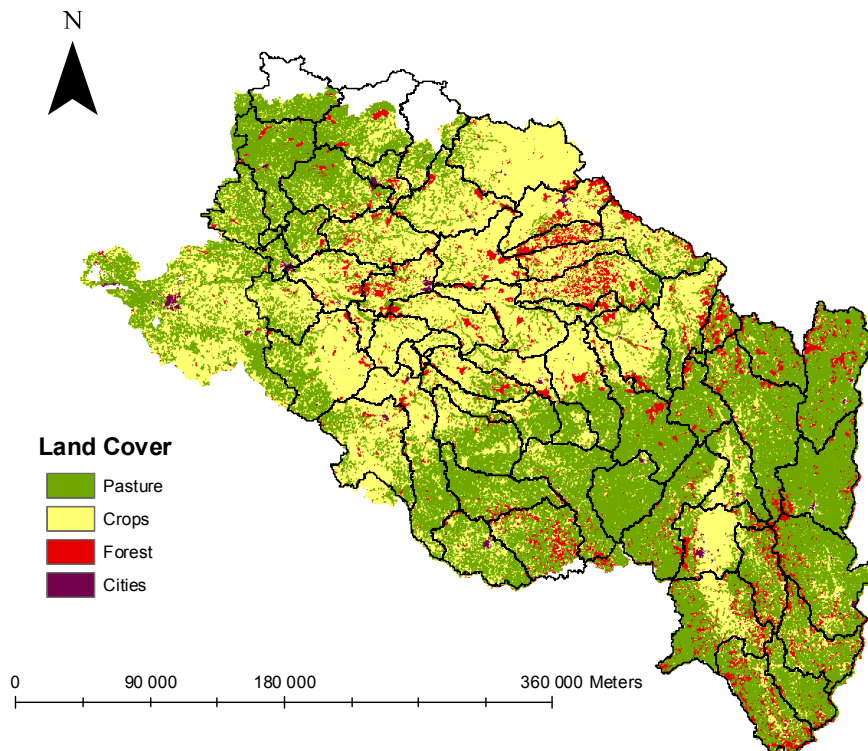


Figure A.3: Map of land use (simplified from the ECOCLIMAP database). Source: V. Bustillo

	River	Area (km <sup>2</sup> )	Cumulated area (km <sup>2</sup> )	Mean elevation (m)	Station	Code	Drainage area (km <sup>2</sup> )
1	La Loire	1327	1327	1068	Loire à Chadrac	K0260010	1308
2	La Loire	1932	3259	940	Loire à Bas-en-Basset	K0550010	3234
3	La Loire	3352	6612	647	Loire à Villerest	K0910010	6585
4	La Loire	2721	9333	436	Loire à Digoïn	K1180010	9315
5	L'Arroux	3166	3166	404	Arroux à Digoïn	K1391810	3166
6	L'Aron	1468	1468	323	Aron à Verneuïl	K1773010	1465
7	La Loire	3662	17629	321	Loire à Nevers	K1930010	17570
8	L'Allier	2263	2263	1067	Allier à Vieille-Brioude	K2330810	2269
9	L'Allier	3117	5379	838	Allier à Vic-le-Comte	K2680810	5370
10	La Dore	1522	1522	767	Dore à Dorat	K2981910	1520
11	L'Allier	2022	8923	520	Allier à Saint-Yorre	K3030810	8940
12	La Sioule	2399	2399	658	Sioule à St Pourçain	K3382010	2458
13	L'Allier	1675	12997	360	Allier à Moulins	K3450810	12980
14	L'Allier	1346	14343	268	Allier à Cuffy	K3650810	14310
15	La Loire	707	32679	295	Loire à Cours-les-Barres	K4000010	32610
16	La Loire	2063	34742	235	Loire à Gien	K4180010	35500
17	La Loire	1763	36505	201	Loire à Orléans	K4350020	36970
18	La Loire	1847	38352	138	Loire à Blois	K4470010	38320
19	Le Cosson	744	744	137	Cosson à Vineuïl	K4783010	702
20	Le Beuvron	1073	1073	145	Beuvron à Tour-en-Sologne	K4672210	1102
21	La Loire	2002	42171	135	Loire à Tours	K4900010	42130
22	Le Cher	1837	1837	525	Cher à Saint-Victor	K5220910	1836
23	Le Cher	1390	3227	350	Cher à St Amand-Montrond	K5400920	3492
24	Le Cher	1303	4530	227	Cher à Foëcy	K5490910	4527
25	L'Arnon	827	827	281	Arnon à St Baudel	K6102420	820
26	L'Arnon	1347	2174	189	Arnon à Méreau	K6192420	2164
27	La Yèvre	1973	1973	208			
28	Le Cher	619	9296	167	Cher à Selles-sur-Cher	K6220910	9252
29	La Sauldre	2284	2284	199	Sauldre à Selles-sur-Cher	K6492510	2254
30	Le Cher	2121	13701	147	Cher à Savonnières	K6720910	13680
31	L'Indre	644	644	318	Indre à Ardentes	K7202610	697
32	L'Indre	1065	1709	173	Indre à Saint-Cyrans	K7312610	1712
33	L'Indre	1623	3332	136	Indre à Bréhémont	K7542610	3284
34	La Loire	821	81136	118			
35	La Vienne	2297	2297	553	Vienne à Palais	L0400610	2296
36	La Vienne	1804	4101	360	Vienne à Etagnac	L0920610	4100
37	La Vienne	1413	5514	233	Vienne à Lussac	L1400610	5535
38	Le Clain	2864	2864	168	Clain à Dissay	L2501610	2886
39	La Vienne	1662	10040	139	Vienne à Ingrandes	L3200610	10050
40	La Creuse	2428	2428	483	Creuse à Eguzon	L4530710	2400
41	La Creuse	913	3341	231	Creuse à Ciron	L4710710	3343
42	La Gartempe	1870	1870	361	Gartempe à Montmorillon	L5411810	1868
43	La Gartempe	2037	3907	209			
44	La Creuse	765	8013	140	Creuse à Leugny	L6020710	8020
45	La Claise	890	890	144	Claise au Grand-Pressigny	L6202030	897
46	La Creuse	363	9265	140			
47	La Creuse	297	9562	127			
48	La Vienne	297	19899	117	Vienne à Nouâtre	L7000610	19920
49	La Vienne	928	20827	113			
50	La Vienne	284	21111	94			
51	Le Thouet	3280	3280	146	Thouet à Chacé	L8602110	3315
52	La Loire	1738	86154	82	Loire à Ponts-de-Cé	L8700010	84809
53	Le Loir	2108	3587	190			
54	La Conie	1479	1479	161	Conie à Conie-Molitard	M1073010	500
55	Le Loir	2335	5922	164	Loir à Flée	M1341610	5940
56	Le Loir	1999	7922	112	Loir à Durtal	M1531610	7925
57	La Sarthe	2711	2711	184	Sarthe à Neuville	M0250610	2716
58	L'Huisne	1915	1915	190	Huisne à Montfort	M0421510	1890
59	La Sarthe	669	5295	120	Sarthe à Spay	M0500610	5285
60	La Sarthe	968	6262	92			
61	La Sarthe	1230	7492	129	Sarthe à Saint-Denis	M0680610	7380
62	La Sarthe	841	16255	68			
63	La Mayenne	1857	1857	222	Mayenne à St Fraimbault	M3230920	1851
64	La Mayenne	2307	4164	144	Mayenne à Chambellay	M3630910	4158
65	L'Oudon	1414	1414	99	Oudon à Andigné	M3861810	1409
66	la Mayenne	124	5702	73	Mayenne à Montreuïl-Juigné	M3910910	5803
67	La Maine	212	22170	67	Maine à Angers	M4101910	22020
68	La Loire	1719	110043	103	Loire à Montjean	M5300010	109930

**Table A.1:** Unit catchments in the Loire River basin and associated gauging stations.

## **A.2 Modelling results**

Nor4: CLSM without LR				R4on: CLSM with or without LR				
	Simulation	$\nu$ (m <sup>-1</sup> )	$\alpha_{K_{mult}}$	Simulation	$\nu$ (m <sup>-1</sup> )	$\alpha_{K_{mult}}$	$\alpha$	$\tau_G$ (days)
1	nor4.g1.k2	1	2	r4on.g2.k2.f0.3.t365	2	2	0.3	365
2	nor4.g3.k2	3	2	nor4.g3.k2	3	2	0	0
3	nor4.g3.k2	3	2	nor4.g3.k2	3	2	0	0
4	nor4.g3.k2	3	2	nor4.g3.k2	3	2	0	0
5	nor4.g2.k2	2	2	nor4.g2.k2	2	2	0	0
6	nor4.g2.k2	2	2	nor4.g2.k2	2	2	0	0
7	nor4.g2.k2	2	2	nor4.g2.k2	2	2	0	0
8	nor4.g2.k2	2	2	nor4.g2.k2	2	2	0	0
9	nor4.g1.k2	1	2	nor4.g1.k2	1	2	0	0
10	nor4.g1.k2	1	2	r4on.g3.k2.f0.2.t182	3	2	0.2	182
11	nor4.g3.k2	3	2	r4on.g3.k2.f0.3.t91	3	2	0.3	91
12	nor4.g3.k2	3	2	nor4.g3.k2	3	2	0	0
13	nor4.g4.k4	4	4	nor4.g4.k4	4	4	0	0
14	nor4.g4.k4	4	4	nor4.g4.k4	4	4	0	0
15	nor4.g2.k2	2	2	nor4.g2.k2	2	2	0	0
16	nor4.g2.k2	2	2	nor4.g2.k2	2	2	0	0
17	nor4.g2.k2	2	2	nor4.g2.k2	2	2	0	0
18	nor4.g2.k2	2	2	nor4.g2.k2	2	2	0	0
19	nor4.g1.k4	1	4	nor4.g1.k4	1	4	0	0
20	nor4.g1.k4	1	4	nor4.g1.k4	1	4	0	0
21	nor4.g2.k2	2	2	nor4.g2.k2	2	2	0	0
22	nor4.g3.k2	3	2	nor4.g3.k2	3	2	0	0
23	nor4.g3.k2	3	2	nor4.g3.k2	3	2	0	0
24	nor4.g2.k2	2	2	r4on.g4.k0.f0.3.t91	4	0	0.3	91
25	nor4.g1.k2	1	2	r4on.g4.k2.f0.8.t91	4	2	0.8	91
26	nor4.g1.k2	1	2	r4on.g2.k4.f1.t730	2	4	1	730
27	nor4.g2.k2	2	2	nor4.g3.k2	3	2	0	0
28	nor4.g4.k4	4	4	nor4.g3.k2	3	2	0	0
29	nor4.g1.k4	1	4	r4on.g1.k4.f1.t91	1	4	1	91
30	nor4.g2.k2	2	2	nor4.g2.k2	2	2	0	0
31	nor4.g2.k2	2	2	nor4.g2.k2	2	2	0	0
32	nor4.g2.k2	2	2	nor4.g2.k2	2	2	0	0
33	nor4.g1.k0	1	0	r4on.g2.k0.f0.8.t730	2	0	0.8	730
34	nor4.g2.k2	2	2	nor4.g2.k2	2	2	0	0
35	nor4.g2.k2	2	2	nor4.g2.k2	2	2	0	0
36	nor4.g2.k2	2	2	r4on.g2.k0.f0.4.t91	2	0	0.4	91
37	nor4.g1.k0	1	0	r4on.g4.k0.f0.4.t182	4	0	0.4	182
38	nor4.g1.k2	1	2	r4on.g2.k2.f0.4.t91	2	2	0.4	91
39	nor4.g2.k2	2	2	nor4.g3.k2	3	2	0	0
40	nor4.g2.k2	2	2	nor4.g2.k2	2	2	0	0
41	nor4.g2.k2	2	2	nor4.g2.k2	2	2	0	0
42	nor4.g2.k2	2	2	r4on.g2.k2.f0.3.t182	2	2	0.3	182
43	nor4.g2.k2	2	2	r4on.g4.k0.f0.3.t182	4	0	0.3	182
44	nor4.g2.k2	2	2	r4on.g4.k0.f0.3.t182	4	0	0.3	182
45	nor4.g2.k2	2	2	r4on.g2.k2.f0.3.t182	2	2	0.3	182
46	nor4.g2.k2	2	2	nor4.g2.k2	2	2	0	0
47	nor4.g2.k2	2	2	nor4.g2.k2	2	2	0	0
48	nor4.g2.k2	2	2	nor4.g2.k2	2	2	0	0
49	nor4.g2.k2	2	2	nor4.g2.k2	2	2	0	0
50	nor4.g2.k2	2	2	nor4.g2.k2	2	2	0	0
51	nor4.g2.k2	2	2	nor4.g2.k2	2	2	0	0
52	nor4.g2.k2	2	2	nor4.g2.k2	2	2	0	0
53	nor4.g1.k2	1	2	r4on.g2.k2.f0.4.t91	2	2	0.4	91
54	nor4.g1.k2	1	2	r4on.g2.k0.f0.9.t730	2	0	0.9	730
55	nor4.g1.k2	1	2	r4on.g2.k2.f0.4.t91	2	2	0.4	91
56	nor4.g1.k0	1	0	r4on.g2.k0.f0.5.t730	2	0	0.5	730
57	nor4.g2.k2	2	2	r4on.g2.k2.f0.3.t91	2	2	0.3	91
58	nor4.g1.k2	1	2	r4on.g2.k2.f0.7.t365	2	2	0.7	365
59	nor4.g1.k0	1	0	nor4.g2.k2	2	2	0	0
60	nor4.g1.k2	1	2	r4on.g2.k0.f0.4.t91	2	0	0.4	91
61	nor4.g1.k2	1	2	r4on.g2.k0.f0.4.t91	2	0	0.4	91
62	nor4.g2.k2	2	2	nor4.g2.k2	2	2	0	0
63	nor4.g1.k2	1	2	r4on.g2.k2.f0.3.t91	2	2	0.3	91
64	nor4.g2.k2	2	2	nor4.g2.k2	2	2	0	0
65	nor4.g2.k2	2	2	nor4.g2.k2	2	2	0	0
66	nor4.g2.k2	2	2	nor4.g2.k2	2	2	0	0
67	nor4.g2.k2	2	2	nor4.g2.k2	2	2	0	0
68	nor4.g2.k2	2	2	nor4.g3.k2	3	2	0	0

**Table A.2:** Selected parameter sets for the two calibrated simulations. Note that  $K_{mult}$  is derived from  $\alpha_{K_{mult}}$ :  $K_{mult} = \sqrt{10^{\alpha_{K_{mult}}}}$ .

Station	$\Delta_{10}$	$Q_{obs}$ ( $m^3 s^{-1}$ )	$Q_{sim}$ ( $m^3 s^{-1}$ )	%BiasR	NS	$\Delta_{10}$	$Q_{obs}$ ( $m^3 s^{-1}$ )	$Q_{sim}$ ( $m^3 s^{-1}$ )	%BiasR	NS	
Calibration period (from August 1976 to July 1992)						Validation period (from August 1992 to July 2007)					
1	Loire à Chadrac	584	15.3	23.1	50.55	0.35	465	13.9	25.3	81.95	-0.28
2	Loire à Bas-en-Basset	584	38.9	52.1	34.12	0.69	547	35.6	56.3	58.27	0.35
3	Loire à Villerest	584	71.7	91.8	28.06	0.71	534	66.4	96.5	45.4	0.47
4	Loire à Digoin	582	98.2	126.3	28.55	0.7	535	87.4	124.5	42.43	0.56
5	Arroux à Digoin	584	42.5	47.2	10.87	0.83	399	33.2	43.4	30.89	0.71
6	Aron à Verneuil	472	21.1	21.9	3.97	0.81	489	17.4	19.7	12.98	0.84
7	Loire à Nevers	473	193.4	218.4	12.95	0.77	547	170.9	220.7	29.1	0.7
8	Allier à Vieille-Brioude	583	30.5	37.5	23.06	0.72	547	26.3	40.2	53.13	0.09
9	Allier à Vic-le-Comte	584	66.2	88.8	34.23	0.65	485	60.8	92	51.18	0.26
10	Dore à Dorat	20	32.5	39.8	22.4	0.78	534	20.1	30.9	53.96	0.47
11	Allier à Saint-Yorre	584	103.3	131	26.83	0.68	539	94.6	136.2	44	0.4
12	Sioule à St Pourçain	546	27	36.2	33.93	0.62	546	24.7	34.9	41.63	0.46
13	Allier à Moulins	584	149.2	182.7	22.46	0.67	517	127	182.7	43.84	0.31
14	Allier à Cuffy	380	188	214.2	13.91	0.74	488	127.5	183.5	43.89	0.28
15	Loire à Cours-les-Barres	544	340.5	421.4	23.75	0.7	541	307.5	422.8	37.49	0.51
16	Loire à Gien	542	377.1	465.5	23.44	0.65	472	309.8	422.8	36.47	0.44
17	Loire à Orléans	584	383	476.4	24.38	0.65	460	328.2	461.6	40.67	0.42
18	Loire à Blois	583	402.2	477.2	18.66	0.65	376	330.1	420.8	27.45	0.53
19	Cosson à Vineuil	0	0	0	0	0	226	3.4	2.2	-37.02	0.43
20	Beuvron à Tour-en-Sologne	344	7.8	4.3	-44.47	0.22	0	0	0	0	0
21	Loire à Tours	255	326.3	377.2	15.59	0.63	358	389	490.4	26.05	0.52
22	Cher à Saint-Victor	0	0	0	0	0	351	18.2	22.6	24.24	0.81
23	Cher à St Amand-Montrond	376	33.9	48.4	42.77	0.69	490	26.1	35.1	34.57	0.77
24	Cher à Foëcy	571	37.6	48.7	29.68	0.74	546	32	42.2	32	0.7
25	Arnon à St Baudel	32	6.3	5.9	-6.68	-0.04	434	4.7	6.9	47.59	0.56
26	Arnon à Méreau	124	18.8	23.8	26.74	0.45	408	13.5	17.1	26.15	0.44
27											
28	Cher à Selles-sur-Cher	547	66.4	81	21.96	0.69	547	65.4	80.8	23.57	0.63
29	Sauldre à Selles-sur-Cher	547	16.6	11.5	-30.63	0.62	542	14.7	13.9	-5.39	0.69
30	Cher à Savonnières	522	112.3	116.2	3.45	0.67	487	86.4	101.7	17.77	0.58
31	Indre à Ardentes	451	6	8.1	33.84	0.75	480	5.6	8.9	57.93	0.55
32	Indre à Saint-Cyrans	499	14.5	14	-2.91	0.86	544	13.4	15.2	13.75	0.74
33	Indre à Bréhémont	51	26.1	34.8	33.48	0.33	0	0	0	0	0
34											
35	Vienne à Palais	584	47.4	48	1.24	0.84	547	47.6	54.3	13.99	0.66
36	Vienne à Etagnac	584	71.6	79.2	10.62	0.85	547	75.3	87.6	16.33	0.71
37	Vienne à Lussac	240	68.2	81.9	19.99	0.8	217	75	91.7	22.26	0.58
38	Clain à Dissay	584	22	24.6	11.86	0.57	462	26.8	23.8	-11.09	0.57
39	Vienne à Ingrandes	584	125.6	128.4	2.18	0.87	547	120.6	133.1	10.35	0.82
40	Creuse à Eguzon	584	30.2	37.7	24.58	0.85	526	27.3	38.9	42.28	0.72
41	Creuse à Ciron	584	40.3	47	16.57	0.86	547	36.6	49	33.74	0.76
42	Gartempe à Montmorillon	584	23.2	27.4	17.87	0.84	363	22.3	28.4	27.04	0.7
43											
44	Creuse à Leugny	584	82.2	97.4	18.44	0.84	547	79.6	99.8	25.37	0.79
45	Claise au Grand-Pressigny	560	4.8	4.9	1.72	0.74	547	4.5	4.9	9.45	0.67
46											
47											
48	Vienne à Nouâtre	584	207.6	235.5	13.42	0.84	547	212.7	242.1	13.82	0.81
49											
50											
51	Thouet à Chacé	540	22.4	21	-6.23	0.72	0	0	0	0	0
52	Loire à Ponts-de-Cé	0	0	0	0	0	4	1168.5	1785	52.76	0.29
53											
54	Conie à Conie-Molitard	270	3.3	3.3	-2.52	-6.99	385	1.7	1.8	5.24	-1.87
55	Loir à Flée	108	42.4	47.2	11.24	0.48	400	25.4	29.2	14.72	0.07
56	Loir à Durtal	474	30.2	40.2	33.01	-0.62	547	35.2	42.3	20.31	0.03
57	Sarthe à Neuville	576	20.4	26.8	31.57	0.72	547	22.4	25.6	14.44	0.78
58	Huisne à Montfort	276	12.1	13.4	10.57	-0.56	547	13.5	16	19.02	-0.4
59	Sarthe à Spay	584	35.8	46.6	30.15	0.41	490	39.8	46.7	17.29	0.44
60											
61	Sarthe à Saint-Denis	584	48.1	60.6	25.99	0.57	547	52.4	61.1	16.72	0.57
62											
63	Mayenne à St Fraimbault	583	18.2	24.3	33.49	0.71	547	22.7	25.1	10.69	0.87
64	Mayenne à Chambellay	584	38.4	44.4	15.6	0.87	547	45.1	46.7	3.49	0.89
65	Oudon à Andigné	408	7.2	8.8	22.4	0.86	270	8.7	10.6	21.47	0.81
66	Mayenne à Montreuil-Juigné	408	44.9	52.5	16.96	0.89	547	54.5	59.7	9.54	0.9
67	Maine à Angers	409	121.8	152	24.72	0.6	547	146.7	167.8	14.35	0.69
68	Loire à Montjean	584	960.8	1062.2	10.56	0.74	547	870.1	1051.5	20.85	0.57

**Table A.3:** Modelling results for the Nor4.g2.k2 simulation.  $\Delta_{10}$ = number of 10-day averages available for comparison at the gauging stations.

Station	$\Delta_{10}$	$Q_{obs}$ ( $m^3 s^{-1}$ )	$Q_{sim}$ ( $m^3 s^{-1}$ )	%BiasR	NS	$\Delta_{10}$	$Q_{obs}$ ( $m^3 s^{-1}$ )	$Q_{sim}$ ( $m^3 s^{-1}$ )	%BiasR	NS	
Calibration period (from August 1976 to July 1992)						Validation period (from August 1992 to July 2007)					
1	Loire à Chadrac	584	15.3	23.2	51.11	0.43	465	13.9	25.6	83.64	0
2	Loire à Bas-en-Basset	584	38.9	52.3	34.55	0.69	547	35.6	56.4	58.37	0.32
3	Loire à Villerest	584	71.7	91.9	28.21	0.72	534	66.4	96.3	45.11	0.4
4	Loire à Digoin	582	98.2	126.2	28.48	0.72	535	87.4	124	41.88	0.49
5	Arroux à Digoin	584	42.5	47.2	10.87	0.83	399	33.2	43.4	30.89	0.71
6	Aron à Verneuil	472	21.1	21.9	3.97	0.81	489	17.4	19.7	12.98	0.84
7	Loire à Nevers	473	193.4	218.2	12.82	0.79	547	170.9	220.2	28.81	0.69
8	Allier à Vieille-Brioude	583	30.5	37.5	23.06	0.72	547	26.3	40.2	53.13	0.09
9	Allier à Vic-le-Comte	584	66.2	88.8	34.11	0.65	485	60.8	92.5	52.07	0.37
10	Dore à Dorat	20	32.5	34.1	5.08	0.76	534	20.1	30.9	53.83	0.46
11	Allier à Saint-Yorre	584	103.3	130.4	26.28	0.68	539	94.6	136.4	44.17	0.46
12	Sioule à St Pourçain	546	27	36.3	34.24	0.64	546	24.7	34.9	41.32	0.38
13	Allier à Moulins	584	149.2	182	22	0.7	517	127	183	44.03	0.39
14	Allier à Cuffy	380	188	213.7	13.64	0.77	488	127.5	183.7	44.03	0.38
15	Loire à Cours-les-Barres	544	340.5	420.1	23.38	0.72	541	307.5	422.2	37.31	0.52
16	Loire à Gien	542	377.1	464.1	23.06	0.68	472	309.8	422.3	36.3	0.46
17	Loire à Orléans	584	383	475.3	24.08	0.68	460	328.2	460.9	40.45	0.44
18	Loire à Blois	583	402.2	476.1	18.38	0.69	376	330.1	420	27.23	0.55
19	Cosson à Vineuil	0	0	0	0	0	226	3.4	4.2	22.62	0.64
20	Beuvron à Tour-en-Sologne	344	7.8	7.5	-3.34	0.74	0	0	0	0	0
21	Loire à Tours	255	326.3	377	15.54	0.65	358	389	495.5	27.37	0.52
22	Cher à Saint-Victor	0	0	0	0	0	351	18.2	22.6	24.22	0.78
23	Cher à St Amand-Montrond	376	33.9	48	41.77	0.7	490	26.1	34	30.34	0.78
24	Cher à Foëcy	571	37.6	48.3	28.58	0.75	546	32	41.4	29.28	0.69
25	Arnon à St Baudel	32	6.3	6	-3.77	0.02	434	4.7	7.2	53.58	0.49
26	Arnon à Méreau	124	18.8	23.7	26.24	0.56	408	13.5	17.8	31.24	0.51
27											
28	Cher à Selles-sur-Cher	547	66.4	81.5	22.8	0.71	547	65.4	80.7	23.32	0.66
29	Sauldre à Selles-sur-Cher	547	16.6	16.8	1.06	0.65	542	14.7	20.8	41.2	0.23
30	Cher à Savonnières	522	112.3	122	8.63	0.68	487	86.4	108.2	25.22	0.58
31	Indre à Ardentes	451	6	8.1	33.84	0.75	480	5.6	8.9	57.93	0.55
32	Indre à Saint-Cyrans	499	14.5	14	-2.91	0.86	544	13.4	15.2	13.75	0.74
33	Indre à Bréhémont	51	26.1	34.4	31.8	0.36	0	0	0	0	0
34											
35	Vienne à Palais	584	47.4	48	1.24	0.84	547	47.6	54.3	13.99	0.66
36	Vienne à Etagnac	584	71.6	79.2	10.62	0.85	547	75.3	87.6	16.33	0.71
37	Vienne à Lussac	240	68.2	80.7	18.3	0.83	217	75	90.1	20.12	0.62
38	Clain à Dissay	584	22	26.2	19.03	0.69	462	26.8	25.4	-5.23	0.71
39	Vienne à Ingrandes	584	125.6	128.9	2.64	0.88	547	120.6	133.5	10.69	0.84
40	Creuse à Eguzon	584	30.2	37.7	24.58	0.85	526	27.3	38.9	42.28	0.72
41	Creuse à Ciron	584	40.3	47	16.57	0.86	547	36.6	49	33.74	0.76
42	Gartempe à Montmorillon	584	23.2	27.4	17.87	0.84	363	22.3	28.4	27.04	0.7
43											
44	Creuse à Leugny	584	82.2	97.4	18.44	0.84	547	79.6	99.8	25.37	0.79
45	Claise au Grand-Pressigny	560	4.8	4.9	1.72	0.74	547	4.5	4.9	9.45	0.67
46											
47											
48	Vienne à Nouâtre	584	207.6	236	13.69	0.85	547	212.7	242.5	14.01	0.82
49											
50											
51	Thouet à Chacé	540	22.4	21	-6.23	0.72	0	0	0	0	0
52	Loire à Ponts-de-Cé	0	0	0	0	0	4	1168.5	1777.4	52.1	0.3
53											
54	Conie à Conie-Molitard	270	3.3	3.3	0.07	-3.94	385	1.7	2.2	27.93	-1.67
55	Loir à Flée	108	42.4	47.7	12.4	0.53	400	25.4	32.8	28.82	0.18
56	Loir à Durtal	474	30.2	42	39.14	-0.18	547	35.2	44.9	27.54	0.12
57	Sarthe à Neuville	576	20.4	26.8	31.57	0.72	547	22.4	25.6	14.44	0.78
58	Huisne à Montfort	276	12.1	14.7	21.57	-0.14	547	13.5	17.5	30.14	0.06
59	Sarthe à Spay	584	35.8	47.4	32.26	0.52	490	39.8	47.9	20.41	0.55
60											
61	Sarthe à Saint-Denis	584	48.1	62.5	29.97	0.65	547	52.4	64.1	22.37	0.65
62											
63	Mayenne à St Fraimbault	583	18.2	24.8	36.77	0.74	547	22.7	26	14.66	0.87
64	Mayenne à Chambellay	584	38.4	45	17.16	0.87	547	45.1	47.6	5.48	0.89
65	Oudon à Andigné	408	7.2	8.8	22.4	0.86	270	8.7	10.6	21.47	0.81
66	Mayenne à Montreuil-Juigné	408	44.9	53.4	18.95	0.88	547	54.5	60.6	11.22	0.9
67	Maine à Angers	409	121.8	157.3	29.13	0.68	547	146.7	174.2	18.71	0.73
68	Loire à Montjean	584	960.8	1075.7	11.96	0.74	547	870.1	1070	22.97	0.58

**Table A.4:** Modelling results for the Nor4 simulation.  $\Delta_{10}$ = number of 10-day averages available for comparison at the gauging stations.

Station	$\Delta_{10}$	$Q_{obs}$ ( $m^3 s^{-1}$ )	$Q_{sim}$ ( $m^3 s^{-1}$ )	%BiasR	NS	$\Delta_{10}$	$Q_{obs}$ ( $m^3 s^{-1}$ )	$Q_{sim}$ ( $m^3 s^{-1}$ )	%BiasR	NS	
Calibration period (from August 1976 to July 1992)						Validation period (from August 1992 to July 2007)					
1	Loire à Chadrac	584	15.3	23.1	50.28	0.49	465	13.9	25.2	81	0.03
2	Loire à Bas-en-Basset	584	38.9	52.2	34.23	0.71	547	35.6	56.2	57.97	0.33
3	Loire à Villerest	584	71.7	91.8	28.05	0.72	534	66.4	96.1	44.84	0.42
4	Loire à Digoin	582	98.2	126.1	28.37	0.72	535	87.4	124	41.92	0.49
5	Arroux à Digoin	584	42.5	47.2	10.87	0.83	399	33.2	43.4	30.89	0.71
6	Aron à Verneuil	472	21.1	21.9	3.98	0.81	489	17.4	19.7	12.99	0.84
7	Loire à Nevers	473	193.4	218	12.75	0.79	547	170.9	220	28.73	0.69
8	Allier à Vieille-Brioude	583	30.5	37.5	23.06	0.72	547	26.3	40.2	53.1	0.09
9	Allier à Vic-le-Comte	584	66.2	88.8	34.11	0.65	485	60.8	92.5	52.04	0.37
10	Dore à Dorat	20	32.5	37	13.88	0.91	534	20.1	31	54.37	0.45
11	Allier à Saint-Yorre	584	103.3	130.4	26.3	0.71	539	94.6	136.6	44.4	0.48
12	Sioule à St Pourçain	546	27	36.3	34.23	0.64	546	24.7	34.9	41.35	0.38
13	Allier à Moulins	584	149.2	182	22	0.72	517	127	183.1	44.14	0.41
14	Allier à Cuffy	380	188	213.6	13.6	0.78	488	127.5	183.8	44.15	0.39
15	Loire à Cours-les-Barres	544	340.5	420.1	23.37	0.72	541	307.5	422.4	37.35	0.53
16	Loire à Gien	542	377.1	464.4	23.13	0.69	472	309.8	422.3	36.32	0.47
17	Loire à Orléans	584	383	475.2	24.06	0.69	460	328.2	460.6	40.35	0.45
18	Loire à Blois	583	402.2	476	18.36	0.69	376	330.1	420.8	27.48	0.56
19	Cosson à Vineuil	0	0	0	0	0	226	3.4	4.2	22.62	0.64
20	Beuvron à Tour-en-Sologne	344	7.8	7.5	-3.35	0.74	0	0	0	0	0
21	Loire à Tours	255	326.3	376.6	15.4	0.65	358	389	494.9	27.2	0.53
22	Cher à Saint-Victor	0	0	0	0	0	351	18.2	22.6	24.2	0.78
23	Cher à St Amand-Montrond	376	33.9	48	41.77	0.7	490	26.1	34	30.33	0.78
24	Cher à Foëcy	571	37.6	47.5	26.37	0.77	546	32	40.4	26.23	0.72
25	Arnon à St Baudel	32	6.3	5.9	-6.52	0.16	434	4.7	7	48.61	0.03
26	Arnon à Méreau	124	18.8	22.2	18.17	0.58	408	13.5	18.6	37.27	0.49
27											
28	Cher à Selles-sur-Cher	547	66.4	80.8	21.62	0.78	547	65.4	79.5	21.48	0.71
29	Sauldre à Selles-sur-Cher	547	16.6	16.9	2.12	0.69	542	14.7	21	42.86	0.36
30	Cher à Savonnières	522	112.3	121.7	8.41	0.73	487	86.4	107.8	24.79	0.64
31	Indre à Ardentes	451	6	8.1	33.84	0.75	480	5.6	8.9	57.93	0.55
32	Indre à Saint-Cyrans	499	14.5	14	-2.91	0.86	544	13.4	15.2	13.75	0.74
33	Indre à Bréhémont	51	26.1	31.6	21.09	0.66	0	0	0	0	0
34											
35	Vienne à Palais	584	47.4	48	1.24	0.84	547	47.6	54.3	13.98	0.66
36	Vienne à Etagnac	584	71.6	78.3	9.31	0.89	547	75.3	86.7	15.09	0.83
37	Vienne à Lussac	240	68.2	78.2	14.66	0.88	217	75	87.6	16.88	0.75
38	Clain à Dissay	584	22	25.1	14.14	0.78	462	26.8	24.3	-9.17	0.77
39	Vienne à Ingrandes	584	125.6	125.6	0.02	0.9	547	120.6	129.7	7.59	0.9
40	Creuse à Eguzon	584	30.2	37.7	24.57	0.85	526	27.3	38.9	42.28	0.72
41	Creuse à Ciron	584	40.3	47	16.57	0.86	547	36.6	49	33.74	0.76
42	Gartempe à Montmorillon	584	23.2	27.4	17.89	0.87	363	22.3	28.3	26.59	0.76
43											
44	Creuse à Leugny	584	82.2	95.4	16.02	0.86	547	79.6	96.7	21.47	0.84
45	Claise au Grand-Pressigny	560	4.8	5	2.4	0.75	547	4.5	4.9	10.17	0.73
46											
47											
48	Vienne à Nouâtre	584	207.6	230.8	11.16	0.89	547	212.7	235.7	10.81	0.88
49											
50											
51	Thouet à Chacé	540	22.4	21	-6.23	0.72	0	0	0	0	0
52	Loire à Ponts-de-Cé	0	0	0	0	0	4	1168.5	1703.4	45.77	0.49
53											
54	Conie à Conie-Molitard	270	3.3	3.6	8.14	-0.93	385	1.7	2.6	50.52	-0.32
55	Loir à Flée	108	42.4	48	13.14	0.73	400	25.4	32.9	29.37	0.48
56	Loir à Durtal	474	30.2	43.3	43.51	0.3	547	35.2	45.5	29.39	0.5
57	Sarthe à Neuville	576	20.4	26.8	31.64	0.74	547	22.4	25.7	14.64	0.78
58	Huisne à Montfort	276	12.1	15.1	24.99	0.5	547	13.5	16.7	24.12	0.66
59	Sarthe à Spay	584	35.8	47.5	32.57	0.69	490	39.8	47.6	19.59	0.72
60											
61	Sarthe à Saint-Denis	584	48.1	61.3	27.48	0.75	547	52.4	61.6	17.53	0.75
62											
63	Mayenne à St Fraimbault	583	18.2	24.3	33.59	0.74	547	22.7	25.1	10.62	0.87
64	Mayenne à Chambellay	584	38.4	44.4	15.65	0.88	547	45.1	46.7	3.45	0.89
65	Oudon à Andigné	408	7.2	8.8	22.4	0.86	270	8.7	10.6	21.47	0.81
66	Mayenne à Montreuil-Juigné	408	44.9	52.7	17.21	0.89	547	54.5	59.7	9.51	0.9
67	Maine à Angers	409	121.8	156.7	28.6	0.76	547	146.7	171.4	16.79	0.8
68	Loire à Montjean	584	960.8	1069.5	11.32	0.77	547	870.1	1059.9	21.81	0.64

**Table A.5:** Modelling results for the R4on simulation.  $\Delta_{10}$ = number of 10-day averages available for comparison at the gauging stations.



# Bibliography

- Bates, B. C., Kundzewicz, Z. W., Wu, S., and Palutikof, J. P.: Climate Change and Water. Technical Paper of the Intergovernmental Panel on Climate Change, IPCC Secretariat, Geneva, 2008.
- Beven, K.: Rainfall-runoff modelling: the primer, John Wiley & Sons Inc, 2001.
- Beven, K. and Binley, A.: The future of distributed models: Model calibration and uncertainty prediction, *Hydrol. Process.*, 6, 279–298, 1992.
- Beven, K. and Freer, J.: Equifinality, data assimilation, and uncertainty estimation in mechanistic modelling of complex environmental systems using the GLUE methodology, *J. Hydrol.*, 249, 11–29, 2001.
- Beven, K. and Kirkby, M. J.: A Physically Based, Variable Contributing Area Model of Basin Hydrology, *Hydrological Sciences Bulletin*, 24, 43–69, 1979.
- Boe, J. and Terray, L.: Uncertainties in summer evapotranspiration changes over Europe and implications for regional climate change, *Geophys. Res. Lett.*, 35, doi:10.1029/2007GL032417, 2008.
- Boe, J., Terray, L., Martin, E., and Habets, F.: Projected changes in components of the hydrological cycle in French river basins during the 21st century, *Water Resour. Res.*, 45, doi:10.1029/2008WR007437, 2009.
- Boone, A., de Rosnay, P., Balsamo, G., Beljaars, A., Chopin, F., Decharme, B., Delire, C., Ducharne, A., Gascoin, S., Grippa, M., Guichard, F., Gusev, Y., Harris, P., Jarlan, L., Kergoat, L., Mougin, E., Nasonova, O., Norgaard, A., Orgeval, T., Ottlé, C., Pocard-Leclercq, I., Polcher, J., Sandholt, I., Saux-Picart, S., Taylor, C., and Xue, Y.: The AMMA Land Surface Model Intercomparison Project, *Bull. Amer. Meteor. Soc.*, doi:10.1175/2009BAMS2786.1, in press, 2009.

- Boone, A., Habets, F., Noilhan, J., Clark, D., Dirmeyer, P., Fox, S., Gusev, Y., Haddeland, I., Koster, R., Lohmann, D., Mahanama, S., Mitchell, K., Nasonova, O., Niu, G., Pitman, A., Polcher, J., Shmakin, A., Tanaka, K., van den Hurk, B., Verant, S., Verseghy, D., Viterbo, P., and Yang, Z.: The Rhone-aggregation land surface scheme intercomparison project: An overview, *J. Clim.*, 17, 187–208, 2004.
- Bustillo, V.: Impact du changement climatique sur l'hydrosystème Loire : HYDROlogie, régime thermique, QUALité (ICC-HYDROQUAL), Phase préliminaire – Travail post-doctoral, 2008.
- Caballero, Y., Voirin-Morel, S., Habets, F., Noilhan, J., LeMoigne, P., Lehenaff, A., and Boone, A.: Hydrological sensitivity of the Adour-Garonne river basin to climate change, *Water Resour. Res.*, 43, doi:10.1029/2005WR004192, 2007.
- Clapp, R. B. and Hornberger, G. M.: Empirical Equations for Some Soil Hydraulic Properties, *Water Resour. Res.*, 14, 601–604, 1978.
- Cosby, B. J., Hornberger, G. M., Clapp, R. B., and Ginn, T. R.: A statistical exploration of the Relationships of Soil Moisture Characteristics to the Physical Properties of Soils, *Water Resour. Res.*, 20, 682–690, 1984.
- Ducharne, A., Bellier, S., Crespi, O., Gascoïn, S., and Zhao, Y.: Validation of a catchment-based land surface model in the Seine River basin (France) using a simple routing model, in prep, 2009a.
- Ducharne, A. et al.: Impact du changement climatique sur les Ressources en Eau et les Extrêmes Hydrologiques dans les bassins de la Seine et la Somme, Rapport final du projet RExHyss, 2009b.
- Ducharne, A., Koster, R. D., Suarez, M. J., Stieglitz, M., and Kumar, P.: A catchment-based approach to modeling land surface processes in a general circulation model 2. Parameter estimation and model demonstration, *J. Geophys. Res.-Atmos.*, 105, 24 823–24 838, 2000.
- Ducharne, A., Baubion, C., Beaudoin, N., Benoit, M., Billen, G., Brisson, N., Garnier, J., Kieken, H., Lebonvallet, S., Ledoux, E., Mary, B., Mignolet, C., Poux, X., Sauboua, E., Schott, C., Thery, S., and Viennot, P.: Long term prospective of the Seine River system: Confronting climatic and direct anthropogenic changes, *Sci. Total Environ.*, 375, 292–311, doi:10.1016/j.scitotenv.2006.12.011, 2007.

- Etchevers, P., Golaz, C., Habets, F., and Noilhan, J.: Impact of a climate change on the Rhone river catchment hydrology, *J. Geophys. Res.-Atmos.*, 107, doi:10.1029/2001JD000490, 2002.
- Famiglietti, J. S. and Wood, E. F.: Multiscale modeling of spatially variable water and energy balance processes, *Water Resour. Res.*, 30, 3061–3078, 1994.
- Gascoïn, S.: Etude des paramétrisations hydrologiques d'un modèle de surface continentale : importance des aquifères et des premiers centimètres du sol, Ph.D. thesis, Université Pierre et Marie Curie - Paris VI, 2009.
- Gascoïn, S., Ducharne, A., Ribstein, P., Carli, M., and Habets, F.: Adaptation of a catchment-based land surface model to the hydrogeological setting of the Somme River basin (France), *J. Hydrol.*, 368, 105–116, doi:10.1016/j.jhydrol.2009.01.039, 2009.
- Gupta, H. V., Beven, K. J., and Wagener, T.: Model Calibration and Uncertainty Estimation, in: *Encyclopedia of Hydrological Sciences*, edited by Anderson, M., pp. 2015–2032, John Wiley & Sons Inc, 2005.
- Henderson-Sellers, A., Yang, Z.-L., and Dickinson, R. E.: The Project for Intercomparison of Land-surface Parameterization Schemes., *Bulletin of the American Meteorological Society*, 74, 1335–1350, doi:10.1175/1520-0477(1993)074, 1993.
- Koster, R. D. and Milly, P. C. D.: The interplay between transpiration and runoff formulations in land surface schemes used with atmospheric models, *J. Clim.*, 10, 1578–1591, 1997.
- Koster, R. D. and Suarez, M. J.: Energy and Water Balance Calculations in the Mosaic LSM, Tech. Rep. 9, NASA Technical Memorandum 104606, 1996.
- Koster, R. D., Dirmeyer, P. A., Guo, Z., Bonan, G., Chan, E., Cox, P., Gordon, C. T., Kanae, S., Kowalczyk, E., Lawrence, D., Liu, P., Lu, C.-H., Malyshev, S., McAvaney, B., Mitchell, K., Mocko, D., Oki, T., Oleson, K., Pitman, A., Sud, Y. C., Taylor, C. M., Verseghy, D., Vasic, R., Xue, Y., and Yamada, T.: Regions of Strong Coupling Between Soil Moisture and Precipitation, *Science*, 305, 1138–1141, doi:10.1126/science.1100217, 2004.
- Koster, R. D., Suarez, M. J., Ducharne, A., Stieglitz, M., and Kumar, P.: A catchment-based approach to modeling land surface processes in a general circulation model 1. Model structure, *J. Geophys. Res.-Atmos.*, 105, 24 809–24 822, 2000.

- Krinner, G., Viovy, N., de Noblet-Ducoudre, N., Ogee, J., Polcher, J., Friedlingstein, P., Ciais, P., Sitch, S., and Prentice, I.: A dynamic global vegetation model for studies of the coupled atmosphere-biosphere system, *Glob. Biogeochem. Cycle*, 19, doi:10.1029/2003GB002199, 2005.
- Kumar, S. V., Reichle, R. H., Peters-Lidard, C. D., Koster, R. D., Zhan, X., Crow, W. T., Eylander, J. B., and Houser, P. R.: A land surface data assimilation framework using the land information system: Description and applications, *Adv. Water Resour.*, 31, 1419–1432, doi:10.1016/j.advwatres.2008.01.013, 2008.
- Longuevergne, L., Gascoïn, S., Boy, J.-P., Rinaldi, S., Ducharne, A., Florsch, N., and Hinderer, J.: Superconducting gravimeter measurements for land surface model assessment, submitted to *GRL*, 2009.
- Mahanama, S. P. P., Koster, R. D., Reichle, R. H., and Zubair, L.: The role of soil moisture initialization in subseasonal and seasonal streamflow prediction - A case study in Sri Lanka, *Adv. Water Resour.*, 31, 1333–1343, doi:10.1016/j.advwatres.2008.06.004, 2008.
- Manabe, S.: Climate and the ocean circulation: 1, the atmospheric circulation and hydrology of the Earth's surface, *Mon. Weather Rev.*, 97, 739–774, 1969.
- Masson, V., Champeaux, J. L., Chauvin, F., Meriguet, C., and Lacaze, R.: A global database of land surface parameters at 1-km resolution in meteorological and climate models, *J. Clim.*, 16, 1261–1282, 2003.
- Milly, P. C. D., Dunne, K. A., and Vecchia, A. V.: Global pattern of trends in streamflow and water availability in a changing climate, *Nature*, 438, 347–350, doi:10.1038/nature04312, 2005.
- Milly, P. C. D., Betancourt, J., Falkenmark, M., Hirsch, R. M., Kundzewicz, Z. W., Lettenmaier, D. P., and Stouffer, R. J.: Climate change - Stationarity is dead: Whither water management?, *Science*, 319, 573–574, doi:10.1126/science.1151915, 2008.
- Monteith, J. L.: Evaporation and environment, in: *Symp. Soc. Exp. Biol*, vol. 19, pp. 205–234, 1965.
- Musy, A. and Soutter, M.: *Physique du sol*, Presses polytechniques et universitaires romandes, 1991.

- Nijssen, B., Bowling, L. C., Lettenmaier, D. P., Clark, D. B., El Maayar, M., Essery, R., Goers, S., Gusev, Y., Habets, F., van den Hurk, B., Jin, J., Kahan, D., Lohmann, D., Ma, X., Mahanama, S., Mocko, D., Nasonova, O., Niu, G., Samuelsson, P., Schmakin, A., Takata, K., Verseghy, D., Viterbo, P., Xia, Y., Xue, Y., and Yang, Z.: Simulation of high latitude hydrological processes in the Torne-Kalix basin: PILPS phase 2(e) - 2: Comparison of model results with observations, *Glob. Planet. Change*, 38, 31–53, doi:10.1016/S0921-8181(03)00004-3, 2003.
- Overgaard, J., Rosbjerg, D., and Butts, M. B.: Land-surface modelling in hydrological perspective - a review, *Biogeosciences*, 3, 229–241, 2006.
- Penman, H. L.: Natural evaporation from open water, bare soil and grass, *Proceedings of the Royal Society of London. Series A, Mathematical and Physical Sciences*, 193, 120–145, 1948.
- Pitman, A. J.: The evolution of, and revolution in, land surface schemes designed for climate models, *Int. J. Climatol.*, 23, 479–510, doi:10.1002/joc.893, 2003.
- Quintana-Segui, P., Le Moigne, P., Durand, Y., Martin, E., Habets, F., Baillon, M., Canellas, C., Franchisteguy, L., and Morel, S.: Analysis of near-surface atmospheric variables: Validation of the SAFRAN analysis over France, *J. Appl. Meteorol. Climatol.*, 47, 92–107, doi:10.1175/2007JAMC1636.1, 2008.
- Reichle, R. H., Crow, W. T., and Keppenne, C. L.: An adaptive ensemble Kalman filter for soil moisture data assimilation, *Water Resour. Res.*, 44, doi:10.1029/2007WR006357, 2008.
- Richards, L. A.: Capillary conduction of liquids in porous media, *Physics*, 1, 318–333, 1931.
- Sellers, P. J., Dickinson, R. E., Randall, D. A., Betts, A. K., Hall, F. G., Berry, J. A., Collatz, G. J., Denning, A. S., Mooney, H. A., Nobre, C. A., Sato, N., Field, C. B., and Henderson-Sellers, A.: Modeling the Exchanges of Energy, Water, and Carbon Between Continents and the Atmosphere, *Science*, 275, 502–509, doi:10.1126/science.275.5299.502, 1997.
- Seneviratne, S. I., Luethi, D., Litschi, M., and Schaer, C.: Land-atmosphere coupling and climate change in Europe, *Nature*, 443, 205–209, doi:10.1038/nature05095, 2006.
- Sivapalan, M., Beven, K., and Wood, E. F.: On Hydrologic Similarity 2. A Scaled Model of Storm Runoff Production, *Water Resour. Res.*, 23, 2266–2278, 1987.

- 
- Wang, A., Bohn, T. J., Mahanama, S. P., Koster, R. D., and Lettenmaier, D. P.: Multimodel Ensemble Reconstruction of Drought over the Continental United States, *J. Clim.*, 22, 2694–2712, doi:10.1175/2008JCLI2586.1, 2009.

# List of Figures

2.1	Illustration of (a) a first-generation land surface model and (b) a second-generation land surface model . . . . .	6
2.2	Vertical representation of soil moisture profile in the CLSM and water fluxes . . . . .	9
2.3	Schematic representation of CLSM spatial partitioning process . . . . .	10
3.1	Map of the Loire River basin . . . . .	15
3.2	Delineation of the 68 unit catchments in the Loire River Basin. . . . .	15
3.3	Location of the gauging stations . . . . .	19
3.4	Scatter plots of efficiency for the Nor4.g2.k2 and the Nor4 simulations . . . . .	20
3.5	Scatter plots of efficiency for the Nor4 and the R4on simulations . . . . .	21
3.6	Comparison between observed and simulated discharges at the outlet of the catchment n°58 during the validation period . . . . .	22
3.7	Scatter plot of efficiency for the R4on simulation . . . . .	23
3.8	Scatter plot of relative bias in total runoff for the R4on simulation . . . . .	23
3.9	Comparison between observed and simulated discharges of the Loire River at Montjean during the validation period . . . . .	25
3.10	Comparison of some hydrological variables from the DEF and the Z2 simulations . . . . .	28
3.11	Comparison in the 68 unit catchments of the occurrences of three different situations . . . . .	30

---

3.12	Comparison between the DEF and the Z2 simulations . . . . .	31
3.13	Comparison between modeled and observed gravity variations in Alsace .	33
3.14	Comparison of some hydrological variables from the DEF, Z2, Z2.pF3 and Z2.pF2.5 simulations . . . . .	35
3.15	Comparison between the DEF, Z2, Z2.pF3 and Z2.pF2.5 simulations . . .	37
A.1	Mean annual precipitation . . . . .	43
A.2	Map of lithology . . . . .	44
A.3	Map of land use cover . . . . .	44

# List of Tables

3.1	Parameter values tested for the CLSM-LR. . . . .	18
3.2	Performance at the basin outlet . . . . .	21
3.3	Performance of the R4on simulation at 11 selected stations . . . . .	24
3.4	Statistics of the soil depth values . . . . .	27
3.5	Annual averages of some variables simulated by the DEF and the Z2 simulations over the Loire River basin during the validation period. . . . .	27
3.6	Statistics of the thresholds values $M_D$ and $M_D^{max}$ . . . . .	29
3.7	Statistics of the wilting point values . . . . .	34
3.8	Annual averages of some variables simulated by the DEF, Z2, Z2.pF3 and Z2.pF2.5 simulations over the Loire River basin during the validation period. . . . .	35
A.1	Characteristics of the 68 unit catchments . . . . .	45
A.2	Selected parameter sets for the two calibrated simulations . . . . .	47
A.3	Modelling results for the Nor4.g2.k2 simulation. $\Delta_{10}$ = number of 10-day averages available for comparison at the gauging stations. . . . .	48
A.4	Modelling results for the Nor4 simulation. $\Delta_{10}$ = number of 10-day averages available for comparison at the gauging stations. . . . .	49
A.5	Modelling results for the R4on simulation. $\Delta_{10}$ = number of 10-day averages available for comparison at the gauging stations. . . . .	50